

A STATISTICAL MODEL OF THE GLOBAL CARBON BUDGET

MIKKEL BENNEDSEN, ERIC HILLEBRAND, AND SIEM JAN KOOPMAN

ABSTRACT.

We propose a dynamic statistical model of the Global Carbon Budget (GCB) as represented in the annual data set made available by the Global Carbon Project (Friedlingsstein et al., 2019, Earth System Science Data 11, 1783–1838), covering the sample period 1959–2018. The model connects four main objects of interest: atmospheric CO₂ concentrations, anthropogenic CO₂ emissions, the absorption of CO₂ by the terrestrial biosphere (land sink) and by the ocean and marine biosphere (ocean sink). The model captures the global carbon budget equation, which states that emissions not absorbed by either land or ocean sinks must remain in the atmosphere and constitute a flow to the stock of atmospheric concentrations. Emissions depend on global economic activity as measured by World gross domestic product (GDP), and sink activity depends on the level of atmospheric concentrations and the Southern Oscillation Index (SOI). We use the model to determine the time series dynamics of atmospheric concentrations, to assess parameter uncertainty, to compute key variables such as the airborne fraction and sink rate, to forecast the GCB components from forecasts of World-GDP and SOI, and to conduct scenario analysis based on different possible future paths of World-GDP.

ACKNOWLEDGMENTS: We are grateful for comments from Søren Johansen, from participants at the fourth conference on Econometric Models of Climate Change in Milan in 2019, the Climate Econometrics Group at Oxford University, in particular Jurgen Doornik, David Hendry, and Felix Pretis. EH posed this modeling problem as Case A of the Econometric Game in 2019 at the University of Amsterdam, and we are indebted to the organizers and participants of the Game. Special thanks go to Peter Boswijk and Joep Keuzenkamp.

1. INTRODUCTION

In this paper, we propose a dynamic statistical model for the time series collected in the annual Global Carbon Budget (GCB), collated and maintained by the Global Carbon Project (Friedlingstein et al., 2019). The model connects atmospheric CO₂ concentrations, anthropogenic emissions, and uptake by the terrestrial biosphere (land sink) and by the ocean and the marine biosphere (ocean sink). It includes the global carbon budget equation as a cornerstone. The model further specifies both sinks as linear in atmospheric concentrations, and it specifies emissions as a random walk with drift, either as a constant or as determined by economic activity. Concentrations are determined by the global carbon budget equation. Since they determine sinks activity in turn, the model captures synchronicity in the determination of key variables.

The model allows for the data-driven study of the global carbon cycle employing a relatively small model. By employing the GCB data set, it facilitates using observational data as well as the output of several large-scale general circulation models (GCM). Parameter uncertainty can be evaluated by way of statistical standard errors, in contrast to GCM or small-scale emulators. On the other hand, the model is limited to the statistical analysis of past data, and all estimated coefficients are obtained from the historical sample, thus in forecasting and scenario analyses the model cannot map substantial changes in technology that would lead to a very different fuel mix globally (see Blanco et al. (2014) for a discussion of the trends in the fuel mix). The model is linear, therefore it incurs approximation errors, for example in the dependence of the sinks on concentrations.

We analyze the time series properties of the components of the GCB. The most conspicuous salient property of all series is that they are upward trending. From a number of unit roots tests and from theoretical relations, we extract a list of requirements that a statistical model of the data has to satisfy. We propose a model that satisfies these requirements, and from its system equations we derive the time series dynamics of atmospheric CO₂ concentrations. This result shows that atmospheric concentrations follow single unit root dynamics that are, however, numerically quite close to a second unit root, and that they approach a second unit root as atmospheric concentrations increase.

We propose and compare two different specifications: The first satisfies the list of requirements and only involves the global time series of the GCB. The second extends the first by including World-GDP as a driver of emissions and by including the Southern Oscillation Index (SOI) as a proxy for the El-Niño/Southern Oscillation (ENSO) cycle in the sinks dynamics. We also include and discuss a number of dummy variables for specific unusual events in the relation of World-GDP and emissions. We present the estimation results and discuss parameter estimation uncertainty.

In simulations of our model, we show the small-sample properties of the statistical estimators and their robustness to the model assumptions. We present and discuss the budget imbalance, the airborne fraction, and the sink rate implied by the models. We conduct a validation experiment where we compute the time series of the GCB using only data on World-GDP and SOI for the last twenty years of the sample, and we show that the model can produce confidence intervals from these two inputs that cover most observations of the GCB components. We nowcast and forecast emissions, sinks activity, and atmospheric concentrations from forecasts of World-GDP and SOI for the period 2019–2021. Finally, we present an analysis of four different scenarios for the path of World-GDP until the year 2100.

The paper is organized as follows. Section 2 introduces the model, discusses central assumptions, and derives a solution for atmospheric concentrations of CO₂ from the system model equations. Section 3 presents Monte Carlo simulation results for the model. Section 4 describes the data set that we use and discusses time series properties of the data series. Section 5 presents estimation results, discusses residual diagnostics, and introduces an extension of the model that includes World-GDP and SOI, including estimation results and residual diagnostics for this extended model. Section 6 discusses limitations of the model as well as the implied budget imbalance, the airborne fraction, and the sink rate. Section 7 presents a validation analysis where the model is estimated on the first 40 years of data and validated on the last 20 years, a forecast exercise for three years out of sample, and scenario analyses until the year 2100. Section 8 concludes.

2. MODEL SPECIFICATION

The statistical global carbon budget (GCB) model proposed in this study is designed for four variables: atmospheric CO₂ concentrations (C_t^*), anthropogenic emissions (E_t^*), CO₂ uptake by the terrestrial biosphere (land sink, $S_LND_t^*$) and CO₂ uptake by the ocean and marine biosphere (ocean sink, $S_OCN_t^*$). The series E_t^* , $S_LND_t^*$, and $S_OCN_t^*$ are measured in gigatons of carbon (GtC) per year; the series C_t^* is measured in GtC. The foundation of our statistical model is the global carbon budget equation

$$(1) \quad G_ATM_{t+1}^* := C_{t+1}^* - C_t^* = E_{t+1}^* - S_LND_{t+1}^* - S_OCN_{t+1}^*,$$

where G_ATM^* represents the growth of atmospheric concentrations. The budget equation expresses that emissions that are not absorbed by either land or ocean sink constitute the annual flow to the stock of atmospheric concentrations. The budget equation further implies a dynamic process for

concentrations as given by

$$C_{t+1}^* = C_t^* + E_{t+1}^* - S_LND_{t+1}^* - S_OCN_{t+1}^*.$$

The dynamic equations for the emission and sink variables are given next. The dynamic evolution of emissions E^* is assumed to follow a random walk process with drift as given by

$$(2) \quad E_{t+1}^* = E_t^* + d + \eta_t^E,$$

with constant drift or growth d and innovation η_t^E . The sinks are assumed to be linear in atmospheric concentrations

$$(3) \quad S_LND_{t+1}^* = c_1 + \frac{\beta_1}{C_{1750}} C_{t+1}^*,$$

$$(4) \quad S_OCN_{t+1}^* = c_2 + \frac{\beta_2}{C_{1750}} C_{t+1}^*,$$

where c_i , $i = 1, 2$, are constant intercepts, and the slopes $\beta_i/C_{1750} > 0$ represent the fractions of concentrations that are absorbed annually by the sinks. We discuss this linearity assumption and the scaling of the parameters by pre-industrial concentrations $C_{1750} = 593.43\text{GtC}$ or 279ppm in the subsections below.

The observed time series for these four variables are denoted with the same variable name but without the asterisk. Annual observations of the four variables at a global level are provided by the Global Carbon Project (Friedlingstein et al., 2019) for the period 1959 through 2018. Atmospheric concentrations are instrumental measurements. Emissions are computed from use of fossil energy carriers as reported by countries' authorities. These observations are typically subject to measurement errors and other irregularities due to data collection. The observations of the land and ocean sinks, on the other hand, are averages over the output of several GCM / Earth system models selected by the Global Carbon Project. We treat these observations statistically as data in our model. However, our statistical model above is formulated as an approximation to the more complex climate models, and it only captures parts of the more detailed interrelations that are defined in the climatologically and mathematically more involved climate models, see the discussions below.

We emphasize that deviations of the observed variables (without asterisk) from the model variables (with asterisk) are therefore a mix of measurement errors (in particular, for concentrations and emissions) and approximation errors (in particular, for land and ocean sink variables). The statistical treatment of GCM model output has received some attention in the recent literature, for example

in Castruccio et al. (2013); Holden et al. (2015); Castruccio and Guinness (2017); Guinness and Hammerling (2018).

Given the dynamic specifications of the key four model variables, we complete the statistical model for the observed variables with the so-called measurement variables

$$(5) \quad C_t = C_t^* + X_{1,t},$$

$$(6) \quad S_LND_t = S_LND_t^* + X_{2,t},$$

$$(7) \quad S_OCN_t = S_OCN_t^* + X_{3,t},$$

$$(8) \quad E_t = E_t^* + X_{4,t},$$

where $X_{1,t}$ and $X_{4,t}$, associated with C_t and E_t , can be mainly regarded as measurement errors and can be treated in the usual way as disturbances, and where $X_{2,t}$ and $X_{3,t}$, associated with S_LND_t and S_OCN_t , mainly represent processes which are not captured by our statistical model.

Under normality assumptions on the innovations η_t^E and the innovations in the X_i processes, the measurement and state equations constitute a linear Gaussian state space model, see the discussion in Appendix A. There, we allow autoregressive processes for the residual processes $X_{i,t}$, for $i = 1, \dots, 4$. We also allow for correlation in the innovations in process X_{it} and in process X_{jt} , denoted r_{ij} , for specific pairs (i, j) . This representation facilitates the estimation of the parameters by the method of maximum likelihood, where the likelihood is evaluated by the Kalman filter, and its maximization relies on a numerical optimization method. The predicted, filtered, and smoothed estimates for the entries of the state vector are obtained by related Kalman filter methods (Durbin and Koopman, 2012). In Section 3, we verify the accuracy of estimation and filtering in a Monte Carlo study, both under correct and incorrect model specifications.

2.1. The land sink as a linear function of atmospheric concentrations. Bacastow and Keeling (1973), p. 94, suggest that the relationship between S_LND_t and atmospheric CO₂ concentrations C_t follows

$$(9) \quad S_LND_t = \beta \log(C_t/C_{1750}),$$

where β is a constant and C_{1750} is the pre-industrial atmospheric concentration. This formula captures the fertilization effect, whereby increased CO₂ concentrations lead to increased net primary

production of plants. A second-order Taylor expansion of this formula in C_{1750} yields

$$(10) \quad S_LND_t \approx \frac{\beta}{C_{1750}}(C_t - C_{1750}) - \frac{\beta}{2C_{1750}^2}(C_t - C_{1750})^2.$$

If $C_t - C_{1750}$ is small relative to C_{1750} , the second-order term is small, and a linear relation between S_LND_t and C_t is a good approximation. If C_t is large relative to C_{1750} , the second-order term becomes important. We can rewrite the Taylor expansion to

$$(11) \quad S_LND_t \approx c_L + k_L(C_t)C_t,$$

where

$$c_L = -\frac{3}{2}\beta, \quad k_L(C_t) = \frac{2\beta}{C_{1750}} - \frac{\beta}{2C_{1750}^2}C_t,$$

and $k_L(C_t)$ is decreasing in C_t . At the beginning of the sample, the atmospheric concentration is $C_{1959} = 670.83\text{GtC}$. The time series of concentrations is then given from the data by

$$C_t = C_{1959} + \sum_{\tau=1959}^t G_ATM_\tau,$$

ending in $C_{2018} = 869.13\text{GtC}$. Therefore, in the beginning of the sample, $k_L(C_{1959}) = 0.0024\beta$, and at the end, $k_L(C_{2018}) = 0.0021\beta$. The assumption of a land sink that grows linearly in concentrations, $k_L(C_t) = k_L$ is thus not unreasonable on the sample. The linearity assumption was suggested already in Bacastow and Keeling (1973), p. 94, and it is discussed and applied, for example, in the context of the airborne fraction and sink rate of CO₂, in Raupach et al. (2014), Raupach (2013), Gloor et al. (2010), Canadell et al. (2007b), and Bennedsen et al. (2019b).

An alternative expression for the fertilization effect was put forward in Gifford (1993):

$$S_LND_t = \frac{a(C_t - C_b)}{1 + b(C_t - C_b)} - 1,$$

where C_b is the atmospheric concentration where net primary production of the terrestrial biosphere is zero ($C_b = 65.9\text{GtC}$ or 31ppm in Gifford (1993), $C_b = 80\text{GtC}$ in Meinshausen et al. (2011)). The parameter b plays a comparable role to the parameter β in the Bacastow-Keeling formula. The parameter a is set in Meinshausen et al. (2011) such that

$$a = \frac{1}{C_{1750} - C_b} + b.$$

This choice neutralizes the intercept term in a Taylor expansion of the formula in C_{1750} , here to second order:

$$\begin{aligned} S_LND_t &\approx \frac{a}{(1+b(C_{1750}-C_b))^2}(C_t-C_{1750}) - \frac{ab}{(1+b(C_{1750}-C_b))^3}(C_t-C_{1750})^2, \\ &\approx k_G(C_t)(C_t-C_{1750}), \end{aligned}$$

and

$$k_G(C_t) = \frac{a}{(1+b(C_{1750}-C_b))^2} - \frac{ab(C_t-C_{1750})}{(1+b(C_{1750}-C_b))^3}$$

decreasing in C_t .

Both the Bacastow-Keeling and the Gifford formulae imply that a regression of S_LND on C_t/C_{1750} and a constant should yield estimated intercepts and regression coefficients that are equal in magnitude with opposite signs, of course up to small sample error. (For the Bacastow-Keeling formula, the first-order term decomposes into $-\beta$ plus $\beta \frac{C_t}{C_{1750}}$, analogously for the Gifford formula.) Table 1 shows that the coefficients are numerically similar in magnitude. The hypothesis that intercept plus slope equal zero cannot be rejected for S_LND . The conclusion from the F tests is not sensitive to whether or not a heteroskedasticity adjustment is applied.

TABLE 1. Simple linear regressions of the sinks series on normalized atmospheric concentrations C_t/C_{1750} . Standard errors in parentheses. F is the F -statistic for a test that intercept plus slope equal zero. $C_{1750} = 593.43$ GtC. The Durbin-Watson statistic indicates first-order serial correlation when it deviates from the benchmark value of 2.

Series	intercept	C_t/C_{1750}	Durbin-Watson	F
S_LND	-5.97 (1.38)	6.41 (1.08)	2.09	1.97 ($p=0.17$)
S_OCN	-5.16 (0.23)	5.43 (0.18)	0.57	19.90 ($p=4e-5$)

2.2. The ocean sink as a linear function of atmospheric concentrations. For the CO₂ flux from atmosphere to ocean, Joos et al. (1996) and Joos et al. (2001) specify the relation

$$S_OCN_t = \tilde{k}_O(pCO2_t^a - pCO2_t^s),$$

where $pCO2_t^a$ and $pCO2_t^s$ are the partial pressures of CO₂ in the atmosphere at sea level and in the ocean surface layer, respectively. The coefficient \tilde{k}_O determines the gas exchange between the atmosphere and the ocean surface layer. The atmospheric partial pressure at sea level is simply a linear transformation of the atmospheric CO₂ concentration. The partial pressure of CO₂ in the

surface layer of the ocean is specified as

$$pCO2_t^s = (pCO2_0^s + \delta_1 \Phi(L) S_OCN_t + \delta_2 [\Phi(L) S_OCN_t]^2 + \dots + \delta_5 [\Phi(L) S_OCN_t]^5) \exp(\gamma(T_t - T_0)),$$

where $pCO2_t^s$ is initial partial pressure in the surface ocean (equal to pre-industrial atmospheric partial pressure assuming equilibrium of the pre-industrial era ocean surface layer with the atmosphere). Since dissolution of CO₂ in the surface ocean depends on temperature, the coefficients $\delta_i = \delta_i(T_0)$ depend on the initial temperature T_0 , and the expression in parentheses is multiplied by an exponential evaluated in the temperature difference $T_t - T_0$ between time t and time 0, multiplied by a coefficient γ . The lag polynomial $\Phi(L)$ is a time-invariant linear filter that describes the dissolution of carbon from the atmosphere in the surface ocean over time:

$$\Phi(L) S_OCN_t = \phi_1 S_OCN_{t-1} + \phi_2 S_OCN_{t-2} + \dots + \phi_{t-1} S_OCN_1.$$

We present the model for an annual sampling frequency. It is specified in Joos et al. (1996) and Joos et al. (2001) for higher resolutions as well, with different $\Phi(L)$ filters for subannual responses, but we abstract from this due to the nature of the data. This model for the ocean sink is employed, for example, in the widely used MAGICC model (Meinshausen et al., 2011). It is clearly a highly nonlinear description of the uptake and dissolution process and how it depends on the pressure differential, the temperature, and temporal dynamics. The key features of the specification for the purposes of our statistical analysis are:

- (1) After suitable unit conversions, the model can be written in the form

$$(12) \quad S_OCN_t = k_O [C_t - C_{1750} - f(\Phi(L) S_OCN_t)],$$

that is, with a leading linear term in current atmospheric CO₂ concentrations.

- (2) Lags of S_OCN_t , and thus lags of C_t , enter into the process both linearly and non-linearly up to fifth powers through function f . This introduces serial correlation (linear terms) and memory in higher moments (non-linear terms). We show in Section 4 that on the data sample, this memory can be sufficiently captured with a linear autoregressive filter of first order, such that the residuals appear as Gaussian white noise.
- (3) The linear specification in the differential of current from initial concentrations is similar to the linearized specification for the land sink. In particular, estimating a linear regression on

C_t/C_{1750} , we expect an estimated intercept of the same magnitude as the regression coefficient, with opposite sign. Table 1 shows that the coefficients are numerically similar in magnitude, but the F test rejects the null hypothesis that their sum is zero. The conclusion does not depend on whether or not a heteroskedasticity adjustment is applied, which is the case here. The Durbin-Watson statistic in the table shows evidence for serial correlation.

2.3. The dynamics of atmospheric concentrations. We assume sinks linear in concentrations, $S_LND_t = k_L C_t + \text{stationary error}$, and $S_OCN_t = k_O C_t + \text{stationary error}$. We employ a random walk with drift for emissions $E_t = d + E_{t-1} + \eta_t^E = E_0 + dt + x_t$, where E_0 are initial emissions, d is the drift term, $x_t = \sum_{\tau=1}^t \eta_{\tau}^E$ and η_t^E is Gaussian white noise for all t . Using the GCB equation

$$\begin{aligned} G_ATM_t &= \Delta C_t = E_t - S_LND_t - S_OCN_t, \\ &= E_0 + dt + x_t - k_L C_t - k_O C_t + \text{stationary error}, \end{aligned}$$

and denoting $q = 1/(1 + k_L + k_O)$, we arrive at a first-order difference equation

$$(1 - qL) C_t = qE_0 + qdt + qx_t + q\varepsilon_t,$$

where ε_t collects the stationary and serially correlated error terms from the two sinks. The deterministic trend and the I(1) process x_t dominate. The difference equation for C_t admits the following solution, where C_0 are initial concentrations,

$$\begin{aligned} (13) \quad C_t &= q^t \left[C_0 - \frac{E_0 q}{1 - q} + \frac{dq^2}{(1 - q)^2} \right] + \left[\frac{E_0 q}{1 - q} - \frac{dq^2}{(1 - q)^2} \right] + \frac{dq}{1 - q} t + \sum_{j=0}^{t-1} q^{j+1} x_{t-j} + \sum_{j=0}^{t-1} q^{j+1} \varepsilon_{t-j}, \\ &= o(1) + O(1) + O(t) + I(1) + I(0) = O(t) + I(1). \end{aligned}$$

Note that the variance of an $I(1)$ process is $O(t)$. The estimated coefficients k_L and k_O are small, from Table 1 we obtain $\hat{k}_L = 6.41/C_{1750} \approx 0.011$ and $\hat{k}_O \approx 5.43/C_{1750} = 0.009$. Thus, the first order polynomial

$$(14) \quad 1 - qz \approx 1 - \frac{1}{1 + 0.011 + 0.009} z$$

has its root $z_0 = 1 + k_L + k_O$ close to, but above, unity. The lag polynomial $1 - qL$ is a stationary filter, but close to simple first differences $1 - L$. Therefore, the term $\sum q^{j+1} x_{t-j}$ is an $I(1)$ process, but close to $I(2)$. Note that the coefficient of the linear trend is $dq/(1 - q) = d/(k_L + k_O)$. This means that the drift dt from emissions is divided by approximately 0.02. This is the reason why the

trend appears dominant in the graph of C_t , even though it is linear. If the lag polynomial was equal to first differences,

$$(1 - L)C'_t = E_0 + dt + x_t + \varepsilon_t,$$

the solution would be

$$C'_t = C_0 + \left[E_0 + \frac{d}{2} \right] t + dt^2 + \sum_{\tau=1}^t x_{\tau} + \sum_{\tau=1}^t \varepsilon_{\tau}.$$

This is a sum of a linear trend, a quadratic trend, an I(2) process, and an I(1) process. In other words, the orders of integration of the terms of the solution (13) would increase by one.

Note that as C_t increases, and thus the distance $C_t - C_{1750}$ from pre-industrial concentrations, the increasingly negative second-order terms in the sink processes move the root of the lag polynomial (14) closer to unity (compare Equation (11)). As terrestrial plants saturate and the ocean acidifies, they take up less CO₂ than at concentrations close to pre-industrial levels (Raupach et al., 2014; Bennedsen et al., 2019b). Therefore, the higher atmospheric concentrations increase, the closer they get to explosive I(2) dynamics.

3. MONTE CARLO SIMULATION STUDY

To validate the maximum likelihood estimation procedure for the unknown parameters in our model, we conduct a Monte Carlo simulation study. We consider the basic model as set out in equations (1) to (8) in the previous section. Given this model specification with a choice of values for the parameter values, which we regard as the “true” model and the “true” parameter values, we simulate data for the time series vector $y_t = (C_t, S_LND_t, S_OCN_t, E_t)'$ from the basic model equations. We notice that for the simulation of y_t , we first need to simulate paths for C_t^* and E_t^* from their dynamic model equations. In a Monte Carlo study of M simulations, we consider each simulated time series vector y_t as an “observed” time series. For each simulated time series, we estimate the “unknown” parameters in the basic model. In this way, we obtain a set of M estimates of the parameter vector. We assess the accuracy of the estimates by comparing the estimated parameter values with the corresponding “true” parameter values. In Table 2 we report the sample bias and standard error for all parameters. The results are based on $M = 1,000$ simulations and on three different time series lengths $T = 50$, $T = 100$ and $T = 250$.

In the description above we consider the same model for simulation as for estimation. Hence we assume correct model specification. The “true” parameter values in this Monte Carlo study are chosen so that they resemble the estimated parameter values from the empirical study in Section 5. Given that our model is linear and Gaussian, and given that exact maximum likelihood estimators

TABLE 2. Results of Monte Carlo Study on Parameter Estimation for Basic Model.

Sample Mean Bias and Sample Standard Error							
true par.	correct spec.	$T = 50$					
		set $\beta_{1,2} = 0$	set $\phi_{1,3} = 0$	set $r_{12,13} = 0$	br G_{ATM}	br Var(η_t)	
$\sigma_{\eta_1}^2$	0.90	-.0203 (.185)	.1060 (.222)	.5313 (.506)	-.0381 (.181)	-.0243 (.183)	.9041 (.409)
$\sigma_{\eta_2}^2$	0.70	-.0074 (.143)	.0118 (.146)	.0008 (.141)	-.0112 (.143)	-.0078 (.142)	.7323 (.324)
$\sigma_{\eta_3}^2$	0.01	-.0005 (.002)	.0003 (.002)	.0059 (.005)	-.0005 (.002)	-.0005 (.002)	.0095 (.005)
$\sigma_{\eta_4}^2$	0.001	.0015 (.003)	.0016 (.003)	.0049 (.008)	.0016 (.003)	.0035 (.006)	.0024 (.004)
$\sigma_{\eta_5}^2$	0.03	-.0032 (.009)	-.0032 (.009)	-.0064 (.008)	-.0033 (.009)	.0551 (.018)	-.0026 (.009)
β_1	7.0	10.42 (69.3)	—	1.851 (18.2)	7.720 (44.3)	1.467 (12.6)	21.43 (110.)
β_2	5.5	.4789 (11.9)	—	-.0539 (7.57)	.4924 (8.60)	.3230 (5.66)	1.785 (26.2)
ϕ_1	0.8	-.0379 (.101)	.0955 (.103)	—	-.0735 (.137)	-.0392 (.102)	-.0403 (.112)
ϕ_3	0.7	-.0584 (.134)	.0546 (.124)	—	-.0611 (.132)	-.0605 (.136)	-.0717 (.143)
r_{12}	-0.65	-.0011 (.086)	.0023 (.085)	.2378 (.108)	—	-.0024 (.086)	.0015 (.099)
r_{13}	-0.15	-.0089 (.108)	-.0159 (.108)	-.0497 (.176)	—	-.0099 (.108)	-.0119 (.115)
$T = 100$							
$\sigma_{\eta_1}^2$	0.90	-.0149 (.129)	.2399 (.268)	.6877 (.468)	-.0236 (.129)	-.0165 (.130)	.9409 (.298)
$\sigma_{\eta_2}^2$	0.70	-.0006 (.101)	.0500 (.131)	.0013 (.100)	-.0012 (.101)	-.0004 (.101)	.7527 (.236)
$\sigma_{\eta_3}^2$	0.01	-.0002 (.001)	.0010 (.002)	.0076 (.004)	-.0002 (.001)	-.0002 (.001)	.0104 (.003)
$\sigma_{\eta_4}^2$	0.001	.0008 (.002)	.0008 (.002)	.0075 (.007)	.0008 (.002)	.0015 (.003)	.0016 (.003)
$\sigma_{\eta_5}^2$	0.03	-.0017 (.006)	-.0018 (.006)	-.0079 (.006)	-.0018 (.006)	.0273 (.010)	-.0012 (.007)
β_1	7.0	.1911 (3.22)	—	-.0835 (3.36)	.2123 (3.83)	.1947 (2.41)	1.240 (17.4)
β_2	5.5	.2068 (2.40)	—	.2222 (2.36)	.2320 (2.41)	-.0552 (1.53)	.3908 (4.03)
ϕ_1	0.8	-.0179 (.056)	.1697 (.055)	—	-.0366 (.078)	-.0194 (.057)	-.0210 (.065)
ϕ_3	0.7	-.0327 (.080)	.1249 (.096)	—	-.0340 (.082)	-.0337 (.080)	-.0390 (.090)
r_{12}	-0.65	.0001 (.060)	.0002 (.065)	.2395 (.074)	—	-.0004 (.060)	.0008 (.068)
r_{13}	-0.15	.0026 (.074)	-.0150 (.076)	-.0383 (.141)	—	.0023 (.074)	.0029 (.082)
$T = 250$							
$\sigma_{\eta_1}^2$	0.90	-.0027 (.080)	.6242 (.456)	.7797 (.333)	-.0057 (.081)	-.0032 (.080)	.9633 (.184)
$\sigma_{\eta_2}^2$	0.70	.0003 (.061)	.1728 (.164)	.0017 (.061)	.0004 (.061)	.0003 (.061)	.7542 (.145)
$\sigma_{\eta_3}^2$	0.01	-.0001 (.001)	.0015 (.001)	.0088 (.003)	-.0001 (.001)	-.0001 (.001)	.0106 (.002)
$\sigma_{\eta_4}^2$	0.001	.0003 (.001)	-.0003 (.001)	.0090 (.004)	.0004 (.001)	.0005 (.002)	.0013 (.002)
$\sigma_{\eta_5}^2$	0.03	-.0008 (.004)	.0004 (.004)	-.0090 (.003)	-.0009 (.004)	.0112 (.005)	-.0005 (.004)
β_1	7.0	.0140 (.555)	—	.0076 (.576)	.0158 (.577)	.0237 (.485)	.0279 (.805)
β_2	5.5	-.0026 (.491)	—	-.0043 (.531)	-.0023 (.493)	-.0228 (.419)	-.0060 (.708)
ϕ_1	0.8	-.0067 (.032)	.1990 (.005)	—	-.0129 (.042)	-.0072 (.032)	-.0082 (.035)
ϕ_3	0.7	-.0121 (.047)	.2065 (.055)	—	-.0124 (.047)	-.0128 (.047)	-.0145 (.052)
r_{12}	-0.65	-.0016 (.036)	-.0432 (.060)	.2321 (.047)	—	-.0016 (.036)	-.0012 (.039)
r_{13}	-0.15	-.0002 (.047)	-.0230 (.050)	-.0356 (.105)	—	-.0004 (.047)	-.0000 (.053)

have good finite sample properties, we expect a good performance overall. However, our study includes small sample cases of $T = 50$ and $T = 100$. In such cases we expect that variances for latent components such as $X_{i,t}$, for $i = 1, \dots, 4$, can be subject to the “pile-up” problem, see the discussions in Shephard (1993) and Stock and Watson (1996). In particular, the “true” variance for $X_{4,t}$ equals 0.001, which is relatively small, and allows this phenomenon to occur. It explains its relatively high bias for small sample sizes. Furthermore, we find that the estimation of the β coefficients in the sink

variables can be challenging in small samples. All other model parameters show good performances with small biases and small standard errors. The bias is measured as the sample mean over the set of M parameter estimates, minus the “true” parameter value. The standard error is based on the corresponding sample variance.

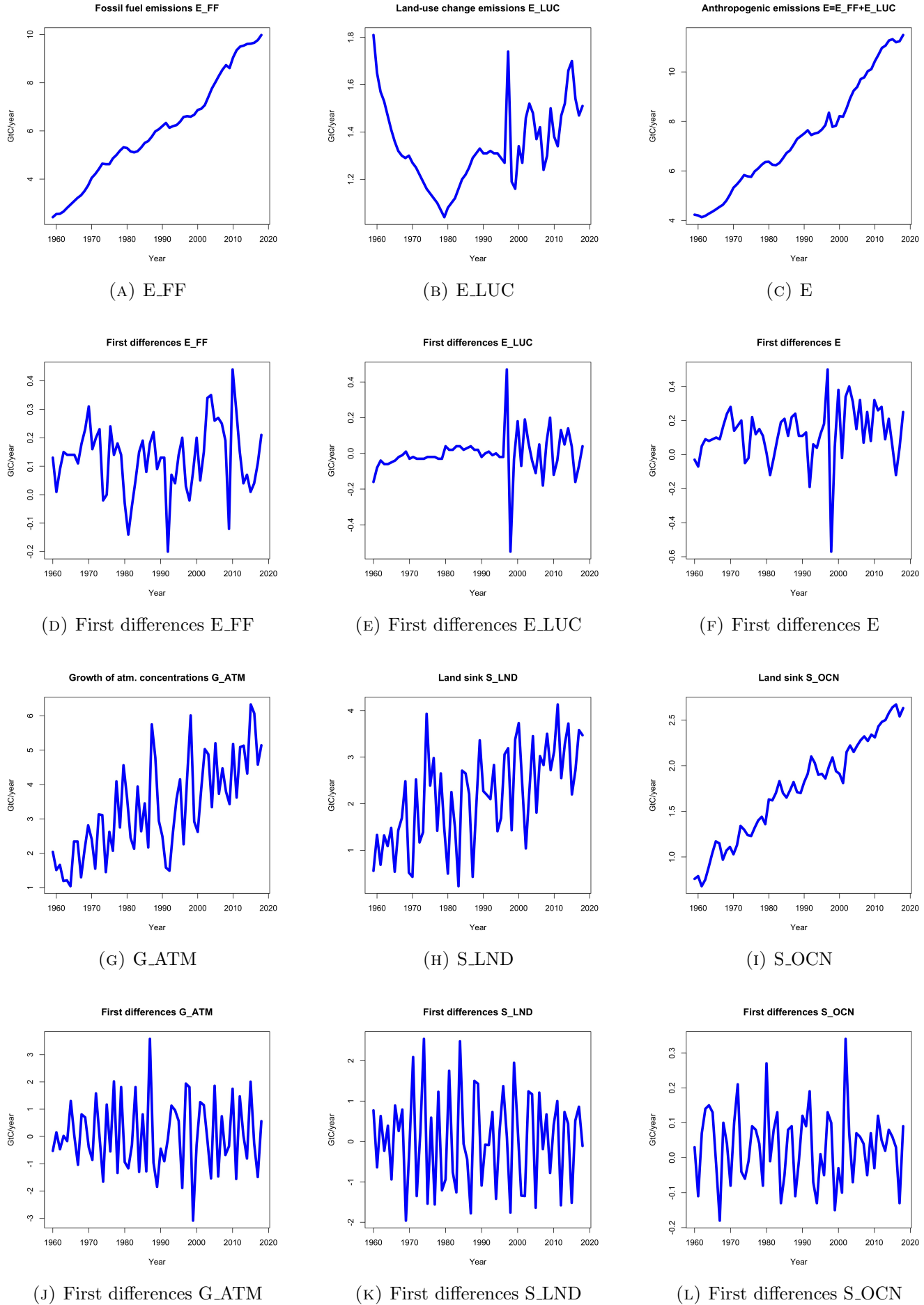
Next, we extend the Monte Carlo study in its assessment of estimation accuracy to cases where the model for the data generation process (DGP) and the model for estimation are different in specific ways. We start by considering cases where we set particular values for the β , ϕ and r_{ij} parameters in the DGP, but we restrict the parameters to zero (as if they were not present in the model) during the subsequent estimation of the remaining parameters. We expect that the estimation of the other parameters will be affected in this erroneous setting: the remaining parameter estimates are subject to the incomplete model specification. Model misspecification affects the estimation accuracy, especially when sample sizes are smaller. However, the model is sufficiently flexible to provide an overall good fit at the cost of increased inaccuracies in the estimation of related parameters.

Finally, we also present results for the case where we distort the DGP model with a structural break in the middle of the time series of the growth term in C_t^* , a one-off change (dummy) in G_ATM_t of 10. In another case we distort the DGP model in the middle of the time series with a change in the variance of $X_{i,t}$ for $i = 1, \dots, 4$; all variances are multiplied by $\sqrt{10}$. For these additional two misspecification cases, the estimation results are also presented in Table 2. The reported biases for these cases show that the break in variance leads to more severe distortions in estimation accuracy.

4. THE DATA SET AND ITS TIME SERIES PROPERTIES

Figure 1 displays the time series from the GCB that we employ in this paper together with their first differences. All series are annual and global and taken from the global file of Friedlingstein et al. (2019), available at <https://www.icos-cp.eu/global-carbon-budget-2019>. All series are measured in gigatons of carbon (GtC) per year. Panel [A] shows fossil fuel emissions E_FF from Gilfillan et al. (2019). Panel [B] shows land-use change emissions E_LUC, which are the average of two series prepared by Houghton and Nassikas (2017) and Hansis et al. (2015). Panel [C] shows the sum of E_FF and E_LUC, labeled anthropogenic emissions E. Panels [D] through [F] show the first differences of the series above. Panel [G] shows growth in atmospheric concentrations, i.e., the first differences of the so-called Keeling curve of atmospheric concentrations (Dlugokencky and Tans, 2019). Panel [H] shows the land sink, which is the mean of the output of 16 different models (Haverd et al., 2018; Melton and Arora, 2016; Lawrence et al., 2019; Tian et al., 2015; Meiyappan et al., 2015;

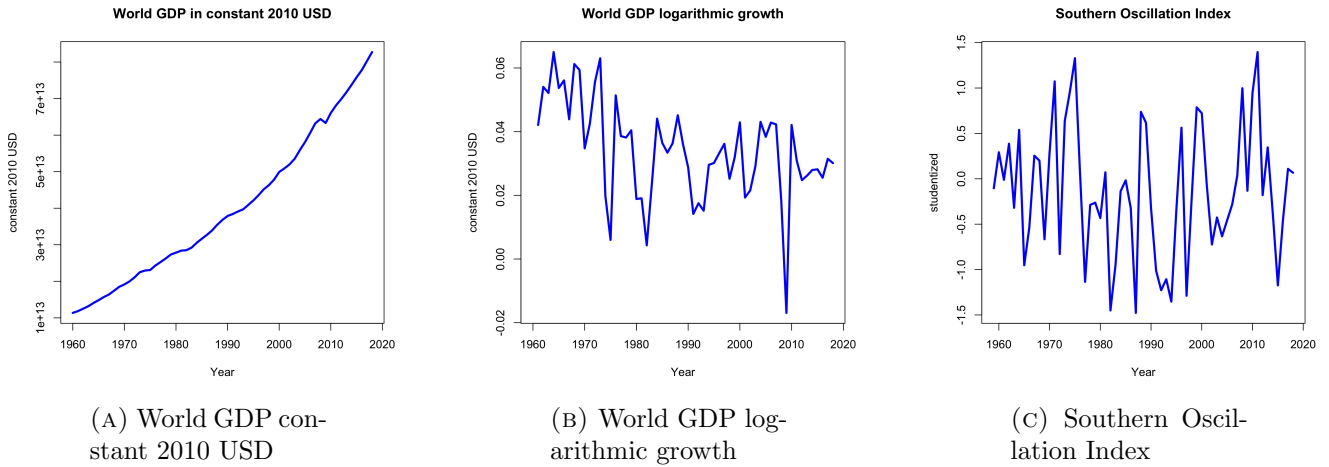
FIGURE 1. GCB time series. E_FF: fossil fuel emissions, E_LUC: land-use change emissions, E: anthropogenic emissions ($E=E_{\text{FF}}+E_{\text{LUC}}$), G_ATM: growth of atmospheric concentrations, S_LND: land sink, S_OCN: ocean sink



Decharme et al., 2019; Mauritzen et al., 2019; Sellar et al., 2019; Smith et al., 2014; Poulter et al., 2011; Lienert and Joos, 2018; Zaehle and Friend, 2010; Goll et al., 2017; Krinner et al., 2005; Walker et al., 2017; Kato et al., 2013). Panel [I] shows the ocean sink, which is the mean of the output of 12 different models (Buitenhuis et al., 2013; Schwinger et al., 2016; Paulsen et al., 2017; Berthet et al., 2019; Law et al., 2017; Hauck et al., 2018; Adcroft et al., 2019; Doney et al., 2009; Aumont et al., 2015; Landschuetzer et al., 2016; Rödenbeck et al., 2014; Denvil-Sommer et al., 2019). Panels [J] through [L] show the first differences of the series above.

Figure 2 displays the time series that are used to extend the model in Section 5. Panel [A] shows World GDP in constant 2010 USD obtained from World Bank (2020b). The year-to-year logarithmic growth rates of World GDP in Panel [B] are employed as drift in the random walk model for emissions. The Southern Oscillation Index (Panel [C]) is used as an additional right-hand side variable for the sinks processes and obtained from Climatic Research Unit (2020); Ropelewski and Jones (1987). The Southern Oscillation Index is the studentized measure of differences in atmospheric pressure at sea level between Tahiti and Darwin, Australia. Positive values correspond to the La Niña phase and negative values to the El Niño phase.

FIGURE 2. World GDP in constant 2010 USD, logarithmic growth rates thereof, Southern Oscillation Index



The most conspicuous feature of the series E_FF, E_G_ATM, S_LND, and S_OCN in Figure 1 is that they are upward trending. E_LUC is the only exception. We conduct augmented Dickey-Fuller (ADF), Phillips-Perron (PP), and Kwiatkowski, Phillips, Schmidt, and Shin (KPSS) tests for unit roots to determine the order of integration of the series and whether stationarity can be achieved by either de-trending or by differencing. We keep the notation of the original sources for each test. The test results are shown in Table 3.

The ADF test regression is given by

$$(15) \quad \Delta y_t = \alpha + \beta t + \pi y_{t-1} + \sum_{j=1}^k \gamma_j \Delta y_{t-j} + u_t,$$

where we select k by Bayes Information Criterion (BIC). We test the hypothesis $H_0 : \pi = 0$ using the t-statistic $\hat{\tau}_\pi$ that follows a Dickey-Fuller distribution (Fuller, 1996, p. 562). If the test rejects and the t-statistic $\hat{\tau}_\beta$ on the trend is insignificant according to a standard t-distribution, the series is stationary. If the test rejects but $\hat{\tau}_\beta$ is significant, the series is trend-stationary. If the test does not reject, the next step is to test the hypothesis $H_0 : (\beta, \rho) = (0, 1)$ in $y_t = \alpha + \beta t + \rho y_{t-1} + v_t$ using the Φ_3 statistic from Dickey and Fuller (1981). If this test rejects, the series is I(1) and the test sequence terminates. If the test fails to reject, we run the ADF test regression

$$(16) \quad \Delta y_t = \alpha + \pi y_{t-1} + \sum_{j=1}^k \gamma_j \Delta y_{t-j} + u_t,$$

where we select k by BIC and test the hypothesis $H_0 : \pi = 0$ using the t-statistic $\hat{\tau}_\mu$ that follows a Dickey-Fuller distribution (Fuller, 1996, p. 562). If the test rejects, the series is stationary. If the test fails to reject, we test the hypothesis $H_0 : (\alpha, \rho) = (0, 1)$ in $y_t = \alpha + \rho y_{t-1} + v_t$ using the Φ_1 statistic from Dickey and Fuller (1981). If the test rejects, the series is I(1) with a drift term (random walk with drift). If the test fails to reject, one continues with an ADF test regression without constant or trend, but this was not the case for any series in the data set.

The Phillips-Perron (PP) test regression is given by

$$(17) \quad y_t = \mu + \beta(t - \frac{1}{2}T) + \alpha y_{t-1} + u_t,$$

where T is the sample size. Phillips and Perron (1988) define a statistic on the α estimate, called $Z(t_{\hat{\alpha}})$ that follows a Dickey-Fuller distribution and is robust to serial correlation in the error term u_t . This obviates the selection of the tuning parameter k in the ADF tests. We test the hypothesis $H_0 : \alpha = 1$ in Equation (17) using $Z(t_{\hat{\alpha}})$. If the test rejects, the series is either stationary or trend-stationary, depending on the test of $H_0 : \beta = 0$ using the $Z(t_{\hat{\beta}})$ statistic proposed in Phillips and Perron (1988). If the test fails to reject, the series is I(1).

The Kwiatkowski et al. (1992) test considers the data-generating model

$$(18) \quad y_t = \xi t + r_t + \varepsilon_t, \quad r_t = r_{t-1} + u_t, \quad u_t \stackrel{i.i.d.}{\sim} N(0, \sigma_u^2),$$

and ε_t stationary. The test is for $H_0 : \sigma_u^2 = 0$, that is, unlike the ADF and Phillips-Perron tests, here the null hypothesis is trend-stationarity. Following Nyblom and Mäkeläinen (1983), Nyblom (1986), and Nabeya and Tanaka (1988), Kwiatkowski et al. consider the locally best invariant statistic

$$(19) \quad LM = \sum_{t=1}^T \left(\sum_{j=1}^t e_j \right)^2 / \hat{\sigma}_\varepsilon^2,$$

where e_j are the residuals from a regression of y_t on an intercept and a trend, and $\hat{\sigma}_\varepsilon^2$ is an estimate of the error variance from this regression. If one wishes to test the null of stationarity instead of trend-stationarity, one simply uses the residuals e_j from a regression on a constant only (distances from the mean). The asymptotic distribution for $\xi = 0$ is a first-level Cramér-von Mises distribution, the asymptotic distribution for $\xi \neq 0$ is a second-level Cramér-von Mises distribution.

Table 3 shows that for E_FF, all tests agree on I(1), the ADF test further specifies a drift term. For E_LUC, the tests disagree, ADF deciding trend-stationarity, PP stationarity, and KPSS I(1). Anthropogenic emissions E inherit the agreement of the tests on E_FF and are clearly I(1), with drift term according to ADF. All tests agree that G_ATM, S_LND, and S_OCN are trend-stationary and that SOI as well as the budget imbalance BIM=E-G_ATM-S_LND-S_OCN are stationary. The KPSS test has marginal room for I(1)-ness of S_OCN, at the 10% level. All tests agree that atmospheric concentrations C are I(1), and G_ATM, which are first differences of C, are unanimously identified as trend-stationary. One might be tempted to conclude from these results that C has a dominant quadratic trend, but this would ignore an important system aspect of the series that we discuss in the next subsection. There is disagreement about Growth in World GDP: ADF decides trend-stationarity, PP stationarity, and KPSS I(1).

The finding that G_ATM, S_LND, and S_OCN are all trend-stationary with upward trends may appear counter-intuitive given that, according to the global carbon budget, the main driver of the system are emissions E. According to the tests presented here, these are a random walk with drift. The drift term in E results in a linear trend, but the deviations from this linear trend are a random walk according to the tests, not a stationary process. The key to understanding the finding is that even though emissions E are cumulated in concentrations, the sinks are subtracted, which are linear in concentrations. This makes for the rich dynamics in equation (13), where we can see that C_t is $O(t) + I(1)$, and thus $\Delta C_t = G_{ATM_t}$ is indeed stationary. The deterministic trend $dt/(k_L + k_O)$ is, however, so dominant in C_t due to the near second unit root that on a small sample of 60 observations, it looks nearly indistinguishable from a quadratic trend and there still seems a linear trend in first differences.

TABLE 3. Unit root tests.

Augmented Dickey-Fuller test: $\hat{\tau}_\tau$ is a statistic from Table 10.A.2 in (Fuller, 1996, p. 642). Φ_3 is the statistic in Table VI in Dickey and Fuller (1981). $\hat{\tau}_\beta$ is the standard t-statistic on the trend coefficient in Equation (15). $\hat{\tau}_\mu$ is a statistic from Table 10.A.2 in (Fuller, 1996, p. 642). Φ_1 is the statistic in Table IV in Dickey and Fuller (1981).

Phillips-Perron test: Both tests are proposed in Phillips and Perron (1988). The $Z(t_{\hat{\alpha}})$ statistic follows the Dickey-Fuller distribution for $\hat{\tau}_\tau$ in Table 10.A.2 in (Fuller, 1996, p. 642). The $Z(t_{\hat{\beta}})$ statistic follows the distribution for $\hat{\tau}_{\beta\tau}$ in Table III in Dickey and Fuller (1981).

KPSS test: The LM statistics are proposed in Kwiatkowski et al. (1992) and described in Equation (19). For LM(trend), the residuals e_j are from a regression on a constant and a trend, for LM(constant), on a constant only.

Series	Augmented Dickey-Fuller test				Phillips-Perron test				KPSS test	
	$\hat{\tau}_\tau$	Φ_3	$\hat{\tau}_\beta$	$\hat{\tau}_\mu$	Φ_1	$Z(t_{\hat{\alpha}})$	$Z(t_{\hat{\beta}})$	Decision	LM(trend)	LM(constant)
E_FF	-1.693 $K=1$	1.488	0.026 $K=1$	7.017***	I(1) w/ drift	-1.581	I(1)	I(1)	0.201**	I(1)
E_LUC	-3.611** $K=1$		2.93*** $K=1$		trend-stationary	-3.93**	2.112	stationary	0.276***	I(1)
E	-1.538 $K=1$	1.432	0.417 $K=1$	10.216***	I(1) w/ drift	-1.966	I(1)	I(1)	0.264***	I(1)
G_ATM	-5.541*** $K=1$		4.146*** $K=1$		trend-stationary	-6.911 ***	5.058***	trend-stationary	0.062	1.259***
C	0.230 $K=1$	9.455*** $K=1$	I(1)			-0.371	I(1)	I(1)	0.373***	trend-stationary
S_LND	-7.042*** $K=1$		4.909*** $K=1$		trend-stationary	-8.113***	4.810***	trend-stationary	0.049	1.245***
S_OCN	-4.416*** $K=1$		4.341*** $K=1$		trend-stationary	-4.109***	3.959***	trend-stationary	0.140*	1.557***
BIM	-4.371*** $K=1$		0.974		stationary	-5.207***	0.090	stationary	0.115	0.114
SOI	-4.957*** $K=1$		0.282		stationary	-5.736***	-0.160	stationary	0.111	0.115
GGDP	-5.348*** $K=1$		-2.081** $K=1$		trend-stationary	-5.349***	-2.528*	stationary	0.163**	I(1)

5. ESTIMATION

The analyses of the dependence of the sink processes on atmospheric concentrations in Sections 2.1 and 2.2, together with the unit root analysis of the constituents of the global carbon budget in Section 4 imply that a statistical model of the GCB needs to have the following properties.

- (1) Emissions E_t follow a random walk plus drift.
- (2) Land and ocean sinks depend linearly on atmospheric concentrations C_t . Since concentrations are monotonically increasing in time, smooth, and only slightly convex on the sample, they are the “trend” that is detected in the unit root tests in Section 4.
- (3) The stationary residual processes X_2, X_3 of the linear relations of the sinks with concentrations should allow for serial correlation, which is in particular expected to be present in the ocean sink.
- (4) Atmospheric concentrations C_t follow a deterministic trend plus I(1) dynamics through the global carbon budget equation.

The model specified in equations (1) to (8), as summarized in the appendix in equation (25), satisfies these properties. In this section, we estimate the model on the Global Carbon Project data set. We discuss residual diagnostics and parameter estimates. We then extend the model to include El-Niño/Southern Oscillation dynamics in the sinks, World-GDP growth in emissions, and a number of dummy variables for outliers in the equation for emissions. We show that extending the model along these three dimensions improves the fit such that residual diagnostics demonstrate that the model describes the data well.

Model (25) can be estimated by standard state space methods. Some state vector elements are diffuse. The estimation results presented here are obtained by maximizing the diffuse log-likelihood via the augmented Kalman filter (Durbin and Koopman, 2012, p. 173). The state vector elements $X_{i,t}$, $i = 1, 2, 3$, are initialized at mean zero and their estimated unconditional variances. Alternatively, the estimation can be run with the standard Kalman filter, initializing the diffuse state vector elements at mean zero and a high variance K , e.g. $K = 1,000,000$. This so-called *Big-K* method yields numerically very similar results. The parameters c_1 , c_2 , and d are added to the state vector, with transition equations that enforce constancy ($\alpha_{i,t+1} = \alpha_{i,t}$ without error term). This is, in essence, a way to concentrate these parameters out of the likelihood. Their estimates and standard errors are returned by the Kalman filter as smoothed state values and (square root of) state variances.

The state equation errors $\eta_t = (\eta_{1,t}, \dots, \eta_{5,t})'$, where $\eta_{5,t} = \eta_t^E$, are assumed to have a covariance matrix that allows for correlations $r_{12}, r_{13} \neq 0$ of $\eta_{1,t}$ (C) with $\eta_{2,t}$ (S_LND) and of $\eta_{1,t}$ (C) with $\eta_{3,t}$ (S_OCN). Estimating a version of the model that allows for the other $r_{ij} \neq 0$ results in estimates that are close to zero and insignificant.

The parameter vector to be estimated by numerical maximum likelihood is thus 11-dimensional:

$$\psi = (\beta_1, \beta_2, \phi_1, \phi_3, \sigma_{\eta_1}^2, \sigma_{\eta_2}^2, \sigma_{\eta_3}^2, \sigma_{\eta_4}^2, \sigma_{\eta_5}^2, r_{12}, r_{13})'.$$

TABLE 4. Residual diagnostics on standardized prediction residuals for model (1) to (8). std dev: standard deviation, skew: skewness, kurt: kurtosis, LB(1) Ljung-Box test statistic for first-order autocorrelation, JB: Jarque-Bera test for normality, DW: Durbin-Watson statistic, *** significant at 0.01-level, ** significant at 0.05-level, * significant at 0.10-level

Residual	mean	std dev	skew	kurt	LB(1)	JB	DW
C	0.030	0.953	0.313	3.061	1.671	0.955	1.659
E	0.204	0.988	-1.372	8.084	0.002	80.66***	1.897
S_LND	-0.152	0.985	0.033	2.960	0.202	0.014	2.064
S_OCN	0.051	0.997	0.263	2.843	0.050	0.729	1.906

Table 4 presents diagnostics on the standardized prediction residuals from the estimation, and Figure 3 shows these residuals together with their correlograms. Table 4 shows that the challenging state vector elements are C and E . The Ljung-Box statistics indicate that there is no serial correlation of first order left in the residuals of any series, but the Durbin-Watson statistic for the residuals from the C equation is some distance from the benchmark value of two, and there are few significant spikes in the partial autocorrelation function in Figure 3, indicating some serial correlation. The Jarque-Bera test of the null of Gaussianity of the residuals from the E equation strongly rejects, driven by both high skewness and leptokurtosis. There is no serial correlation left in the residual from E , on the other hand, as the diagnostic statistics and the correlogram show. The diagnostic statistics for the residuals of the S_LND and S_OCN equations show a good fit in Table 4, but the correlogram in Figure 3 shows some significant spikes at higher lags for the S_LND equation.

Table 5 displays the estimated parameter values and their standard errors. Figure 4 shows the smoothed states, with the data plotted for comparison where available (C, G_ATM, E, S_LND, S_OCN). The correlations of the errors in the state equations are estimated as parameters $r_{12} = \text{corr}(\eta_{1,t}, \eta_{2,t})$ (X_1 [C] with X_2 [S_LND]) and $r_{13} = \text{corr}(\eta_{1,t}, \eta_{3,t})$ (X_1 [C] with X_3 [S_OCN]).

Again, we note the pattern of intercept and slope coefficients of same order of magnitude with opposite signs in the sinks processes (compare with Table 1, where this result was foreshadowed in

FIGURE 3. Standardized prediction residuals for model (1) to (8), ACF autocorrelation function, PACF partial autocorrelation function. Note that the ACF shows the value for lag zero (equal to one by definition), while the PACF does not.

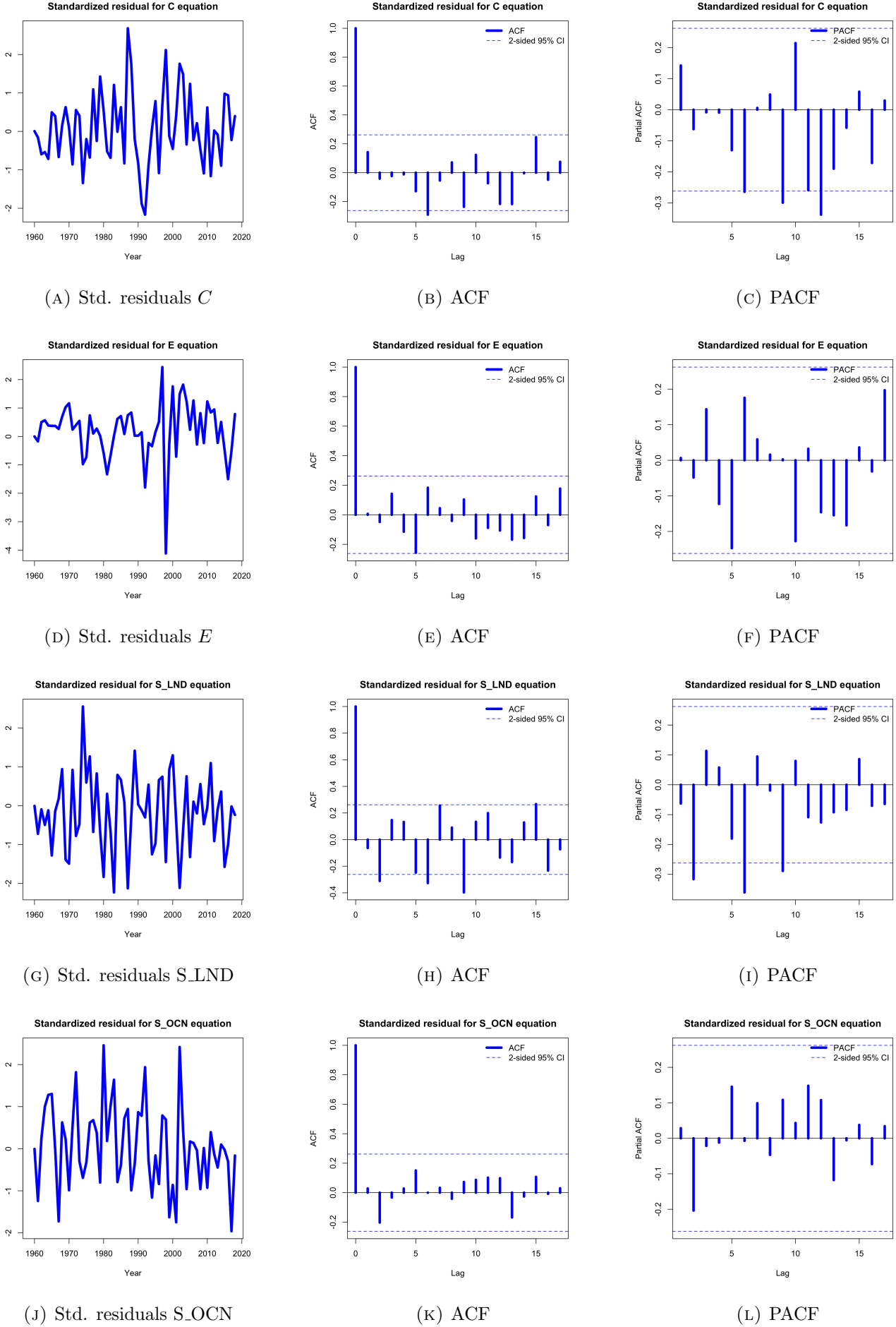


TABLE 5. Parameter estimates for model (1) to (8). std err: standard error, filt.: filtered, i.e., estimated as element of state vector. The numerical maximum likelihood is -62.81.

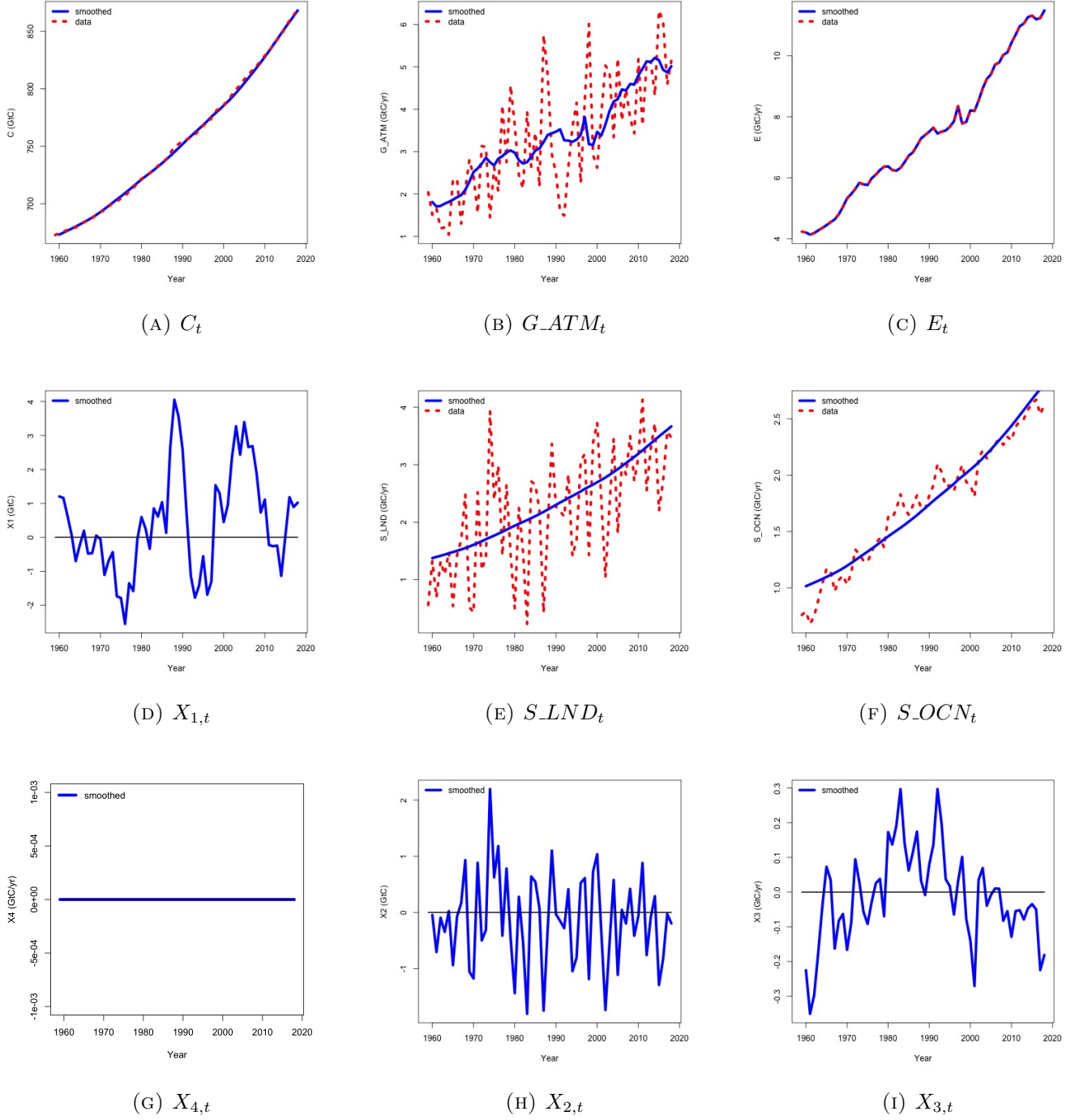
	Coefficients		Variances		
	estimate	std err	estimate	std err	
c_1 (filt.)	-6.90	0.05	$\sigma_{\eta_1}^2$	0.92	0.21
c_2 (filt.)	-5.30	0.04	$\sigma_{\eta_2}^2$	0.68	0.15
β_1	7.23	0.88	$\sigma_{\eta_3}^2$	0.010	0.002
β_2	5.53	0.51	$\sigma_{\eta_4}^2$	3e-08	8e-07
d (filt.)	0.12	0.02	$\sigma_{\eta_5}^2$	0.026	0.004
ϕ_1	0.85	0.08	r_{12}	-0.68	0.08
ϕ_3	0.74	0.09	r_{13}	-0.15	0.12

simple regressions). Figure 4 shows in panels [E] and [F] that the sinks processes are upward trending with slight positive curvature since they are scaled concentrations (panel [A]). The sinks data then exhibit stationary variations around these trends. This is the reason why the unit roots tests in Section 4 identified these time series as trend-stationary.

The serial correlation in the error process $X_{1,t}$ (in C) and $X_{3,t}$ (in S_OCN) is reflected in the estimated autoregressive parameters $\hat{\phi}_1 = 0.85$ and $\hat{\phi}_3 = 0.74$, respectively. These estimates imply substantial serial correlation, but they are far from unity and thus these are clearly stationary processes. The smoothed values of the processes are shown in panels [D] and [H] of Figure 4, where the memory in the series can be seen. The process $X_{2,t}$, on the other hand, is indistinguishable from white noise, and the diagnostics on S_LND in Table 4 show that this is a sufficient description of the data. A version of the model with an additional parameter ϕ_2 to be estimated resulted in a small and insignificant estimate. The process $X_{4,t}$ in the measurement equation of E is estimated to be essentially zero, as shown in Figure 4 (panel [G]), meaning that the random walk with drift for E^* in equation (2) is a sufficient description of the data, and $X_{4,t}$ can be omitted. The average growth in emissions is $\hat{d} = 0.12$ GtC/year. There is a strong correlation between the innovations in the X_1 residual process in C and in the X_2 residual process in S_LND. This may reflect that the models that generate S_LND are calibrated to agree with the concentration measurements (Friedlingstein et al., 2019).

Even though the residual diagnostics on the equations for the sinks do not indicate statistical problems with their fits, a model that reduces them to scaled concentrations seems simple. Since these time series are not measurements but model output, the variations around the trend given by concentrations are meaningful. In a statistical model such as (1) to (8), we cannot capture the rich dynamics of the dynamic global vegetation models or Earth system models behind the S_LND series.

FIGURE 4. Smoothed values for state vector elements of model (1) to (8)



One major determinant of the dynamics beyond concentrations is the El Niño/Southern Oscillation cycle, however, and there are observational data available for this cycle (Climatic Research Unit, 2020; Ropelewski and Jones, 1987). We include a measure of ENSO in the sinks processes, and we opt for the Southern Oscillation Index (SOI). We have also estimated versions that include Niño 3.4 and Oceanic Niño Indices, and the results were very similar, likely because our model is specified for an annual sampling frequency, where the differences between the indices do not matter as much.

In Bennedsen et al. (2019a), we have shown that U.S. CO₂ emissions can be modeled and forecast by industrial production indices. Following Raupach et al. (2007), Friedlingstein et al. (2019) and earlier vintages of the GCB (Le Quéré et al., 2018, 2017) model and forecast emissions by measures of gross domestic product (GDP). The energy economics literature has discussed the relation of energy consumption and macroeconomic activity at length (e.g., Stern, 1993, 2000; Oh and Lee, 2004; Lee, 2005; Zhang and Cheng, 2009; Ozturk, 2010). We therefore replace the constant drift d in equation (2) for E by a coefficient times logarithmic differences in the World Bank's World-GDP series in constant 2010 Dollars (Series ID NY.GDP.MKTP.KD). Simply adding a coefficient times logarithmic growth in World GDP to the constant drift d results in an insignificant estimated constant of $\hat{d} = 0.01$ with a standard error of 0.04 and a significant estimated coefficient on logarithmic differences of World GDP of 3.42 with a standard error of 1.22. The mean logarithmic difference of World GDP on the sample is 3.4% per year, thus $3.42 * 0.034 \approx 0.12$ corresponds to the magnitude of \hat{d} in Table 5. The data thus clearly prefer logarithmic growth of World GDP as the time-varying drift in the random walk for E.

We include four dummy variables in the mean equation and one in the variance of the error term for emissions E*. The selection of the dummies was conducted using a variety of methods and criteria. The point of departure was a purely data-driven search with AutoMetrics (Doornik, 2009; Pretis et al., 2018). The set of selected dummies was modified by a search with the following criteria: (1) The number of dummies should be minimal. (2) The dummies should have an identifying event or narrative. (3) The dummies should be statistically significant at least at the 10% level. (4) The numerical maximum likelihood should be reasonably close to the highest value we saw in all of our experiments. (5) The residual diagnostics as well as the filtered and smoothed states and disturbances should be reasonable.

The final set of dummy variables in the equation for E* contains: (1) 1973 in mean: The first oil price shock is associated with a decrease in emissions. (2) 1980 in mean: The second oil price shock in 1979 and the outbreak of the Iran-Iraq war in 1980 are associated with a decrease in emissions. (3) 1991 in mean: The 1990 oil price shock and the first Gulf War in 1991 are associated with a decrease. The relation between oil price crises, energy consumption, and macroeconomic activity has been discussed at length in the econometrics and energy economics literature, see, e.g., Hamilton (1983); Perron (1989); Hamilton (1996, 2003); Barsky and Kilian (2004); Kilian (2008, 2009); Stern and Kander (2012). (4) 1996 in variance: Panels [D], [E], and [F] of Figure 1 show that first differences of E inherit an increase in variance from first differences of E_LUC in 1996. This change in variance

in E_LUC is displayed in both source time series (Houghton and Nassikas, 2017; Hansis et al., 2015). (5) 1997 in mean: There is a strong spike in levels of E in 1997 due to burning of South East Asian peatlands (Houghton and Nassikas, 2017). The upward spike in levels corresponds to a pulse in first differences, of which the dummy captures the downward movement. We have estimated an alternative specification with a 1997 dummy in the measurement equation instead, but the residual diagnostics favor the inclusion in the state equation for E^* .

We arrive at the following extended specification of the model: The state equations become

$$(1.1') \quad C_{t+1}^* = C_t^* + G_ATM_{t+1}^*,$$

$$(1.2') \quad G_ATM_{t+1}^* = E_{t+1}^* - S_LND_{t+1}^* - S_OCN_{t+1}^*,$$

$$(2') \quad E_{t+1}^* = E_t^* + \beta_5 \Delta \log GDP_{2010,t+1} + \beta_6 I1973 + \beta_7 I1980 + \beta_8 I1991 + \beta_9 I1997 + \eta_{4,t},$$

$$(3') \quad S_LND_{t+1}^* = c_1 + \frac{\beta_1}{C_0} C_{t+1}^* + \beta_3 SOI_{t+1},$$

$$(4') \quad S_OCN_{t+1}^* = c_2 + \frac{\beta_2}{C_0} C_{t+1}^* + \beta_4 SOI_{t+1}.$$

where $\eta_{4,t} = \eta_t^E \sim N(0, \sigma_{\eta_4}^2 * (s_E^2 I_{t \geq 1996}))$, which captures the change in variance in the E residuals.

The measurement equations (5) to (8) become

$$(5') \quad C_t = C_t^* + X_{1,t},$$

$$(6') \quad S_LND_t = S_LND_t^* + X_{2,t},$$

$$(7') \quad S_OCN_t = S_OCN_t^* + X_{3,t},$$

$$(8') \quad E_t = E_t^*,$$

where we have removed the $X_{4,t}$ process from the equation for E based on the results in the first model. The residual processes are given by

$$X_{1,t+1} = \phi_1 X_{1,t} + \eta_{1,t+1},$$

$$X_{2,t+1} = \eta_{2,t+1},$$

$$X_{3,t+1} = \phi_3 X_{3,t} + \eta_{3,t+1},$$

where $\eta_{i,t} \sim N(0, \sigma_i^2)$ for $i = 1, 2, 3$.

The new parameters $\beta_3, \beta_4, \dots, \beta_9$ can all be concentrated out of the likelihood by defining them as constant state variables. This leaves s_E as the only parameter to be added to the vector to be

estimated by maximum likelihood:

$$\psi' = (\beta_1, \beta_2, \phi_1, \phi_3, \sigma_{\eta_1}^2, \sigma_{\eta_2}^2, \sigma_{\eta_3}^2, \sigma_{\eta_4}^2, r_{12}, r_{13}, s_E)',$$

which is still 11-dimensional, since $\sigma_{\eta_5}^2$ has been removed.

TABLE 6. Residual diagnostics on standardized prediction residuals for model (1.1') to (8'). std dev: standard deviation, skew: skewness, kurt: kurtosis, LB(1) Ljung-Box test statistic for first-order autocorrelation, JB: Jarque-Bera test for normality, DW: Durbin-Watson statistic, *** significant at 0.01-level, ** significant at 0.05-level, * significant at 0.10-level

Residual	mean	std dev	skew	kurt	LB(1)	JB	DW
C	-0.031	0.879	-0.239	3.666	0.212	1.569	1.836
E	0.592	0.769	0.351	3.147	1.880	1.198	1.636
S_LND	-0.074	0.983	0.042	2.343	0.478	1.023	2.172
S_OCN	0.032	0.961	0.135	3.441	0.242	0.622	2.093

Table 6 and Figure 5 show residual diagnostics for model (1.1') to (8'). There is no evidence of non-normality remaining in the standardized prediction residuals, and only weak evidence of serial correlation in the C and E equations as measured by the Durbin-Watson statistic. The correlograms in Figure 5 show no evidence of serial correlation. All autocorrelation coefficients for the sinks processes, in particular, are far below the significance bands. We conclude that model (1.1') to (8') describes the data well.

Table 7 reports the parameter estimates of model (1.1') to (8') and Figure 6 shows the smoothed states, together with the data series for comparison, where available. In Table 7, the basic patterns we have described above for Table 5 remain. The coefficients pertaining to SOI in the sink processes are highly significant. They are of opposite sign: La Niña phases (positive SOI) correspond to higher land uptake whereas they correspond to lower ocean uptake. This is to be expected, see, for example, Feely et al. (1999); Haverd et al. (2018). The increase in variance of $\eta_4 = \eta^E$ in 1996 is highly significant and more than quintuples the pre-1996 variance. The dummy variables in the mean of E are all of the expected sign, 1973 is not significant, but it is important for the Jarque-Bera statistic, 1997 is the largest in magnitude. Figure 6 shows that the inclusion of SOI in the sinks makes them much more dynamic, and they trace the data better. G_ATM inherits the enhanced dynamics and also presents a better fit.

6. DISCUSSION

6.1. Limitations. Section 2 discussed common models for the sink processes and how they can be approximated by specifications that are linear in concentrations (Bacastow and Keeling, 1973; Gifford,

FIGURE 5. Standardized prediction residuals for model (1.1') to (8'), ACF autocorrelation function, PACF partial autocorrelation function. Note that the ACF shows the value for lag zero (equal to one by definition), while the PACF does not.

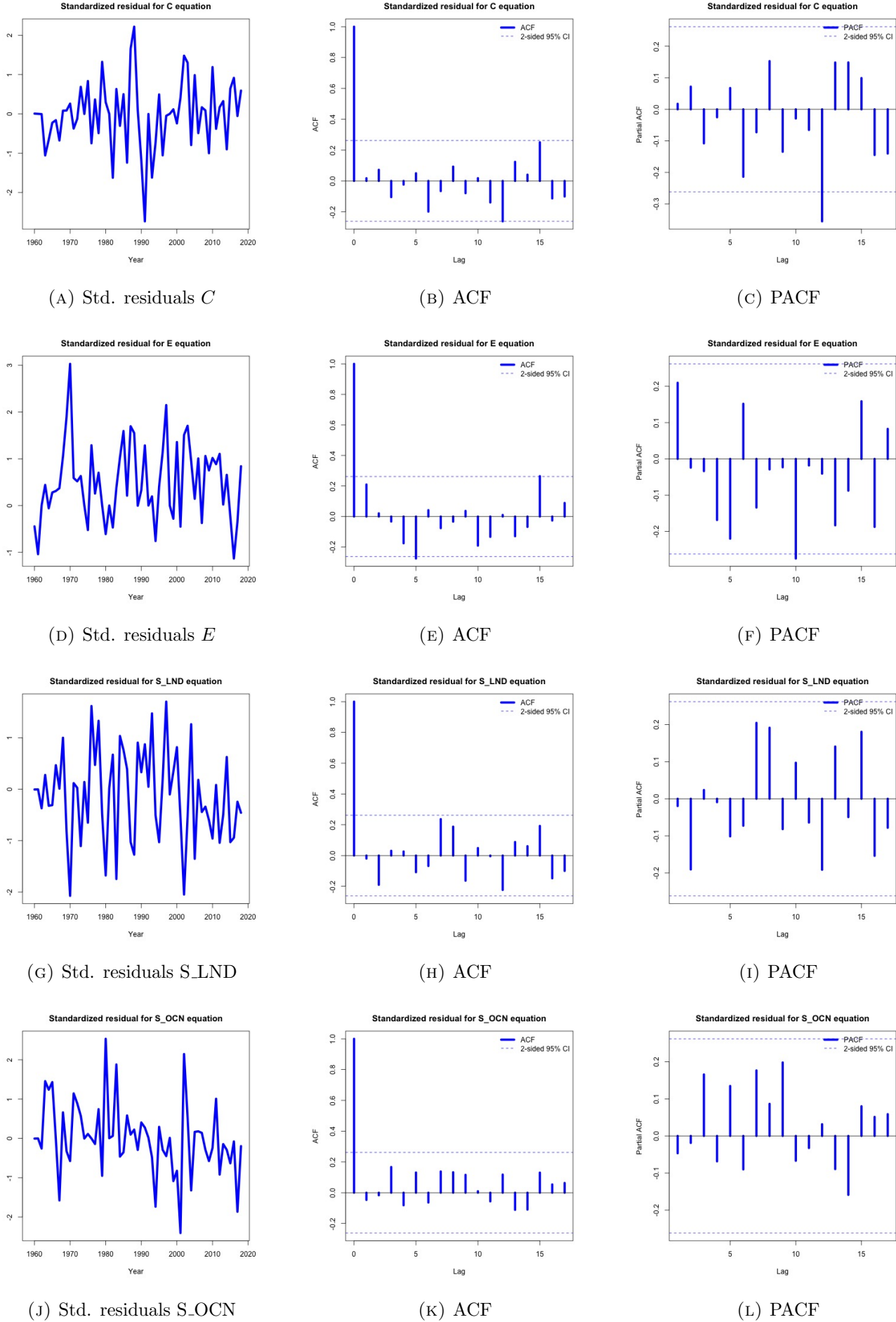


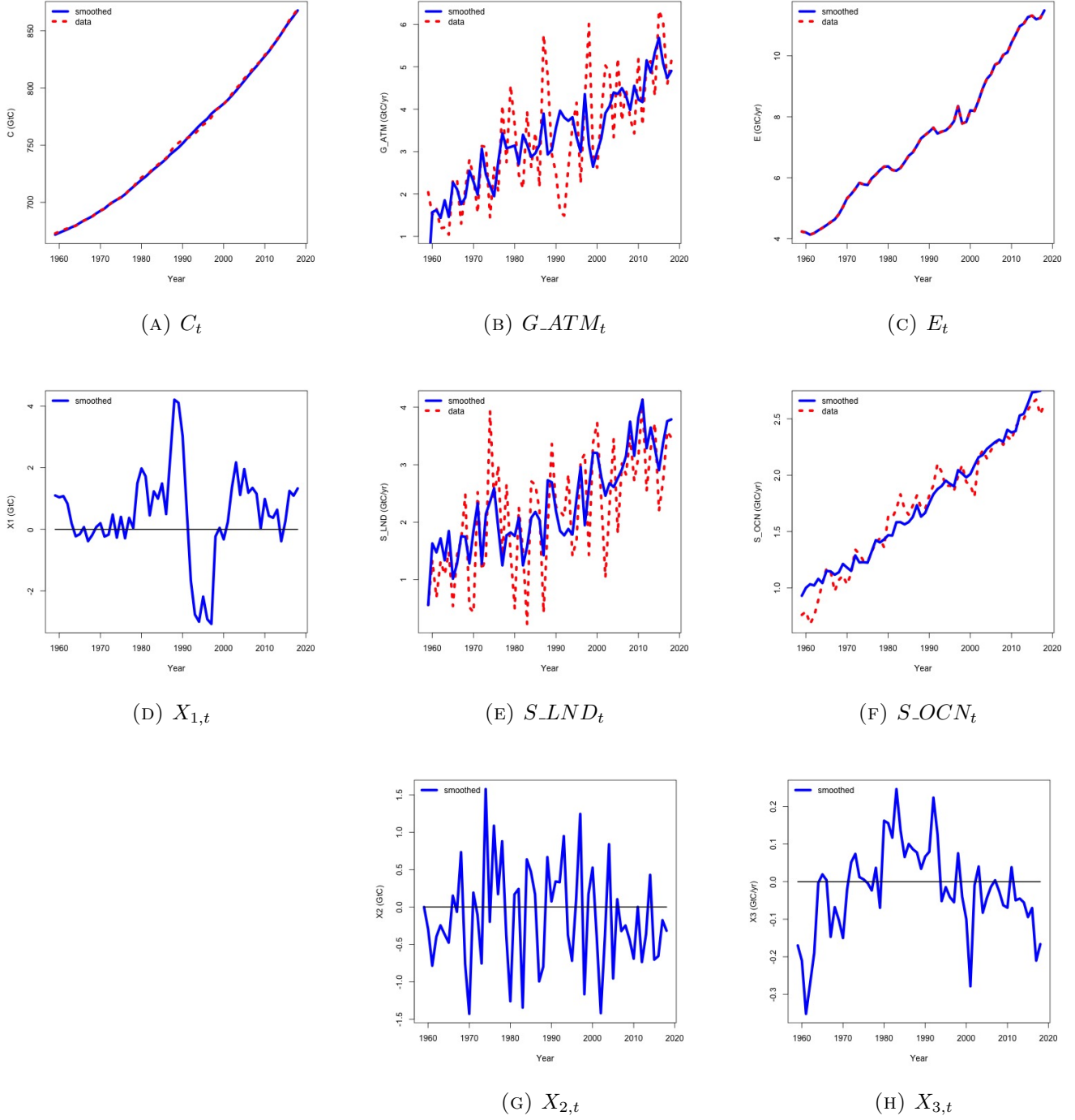
TABLE 7. Parameter estimates for model (1.1') to (8'). std err: standard error, filt.: filtered, i.e., estimated as element of state vector. The numerical maximum likelihood is -43.83.

	Coefficients		Variances		
	estimate	std err	estimate	std err	
c_1 (filt.)	-6.77	0.05	$\sigma_{\eta_1}^2$	0.83	0.20
c_2 (filt.)	-5.35	0.04	$\sigma_{\eta_2}^2$	0.49	0.16
β_1	7.20	0.90	$\sigma_{\eta_3}^2$	0.008	0.002
β_2	5.57	0.48	$\sigma_{\eta_4}^2$	0.006	0.002
β_3 (filt.)	0.57	0.12	r_{12}	-0.63	0.15
β_4 (filt.)	-0.05	0.01	r_{13}	-0.08	0.13
β_5 (filt.)	3.15	0.30	s_E	2.38	0.57
β_6 (filt.)	-0.11	0.08			
β_7 (filt.)	-0.18	0.08			
β_8 (filt.)	-0.25	0.08			
β_9 (filt.)	-0.65	0.18			
ϕ_1	0.86	0.07			
ϕ_3	0.74	0.11			

1993). This means, on the other hand, that there is approximation error in the sink processes in Equations (3') and (4'). The residual diagnostics are encouraging in the sense that there is little evidence of serial correlation remaining, but this may change as new data with higher atmospheric concentrations are observed, which will increase the influence of second-order terms in the Taylor approximations in equations (10) and (12). Also, dependence in higher moments cannot be detected with these measures of linear dependence.

Since model parameters are estimated on the historical sample, they necessarily reflect the technological conditions that prevailed during the sample period. Forecasts or scenario analyses conducted with the model write these technological conditions forth through the use of the estimated parameters. This holds in particular for the fuel mix that is behind emissions E (Friedlingstein et al., 2019, e.g.). Model (1.1') to (8') can thus not shed any light on the effects of changes in the energy mix to, say, higher shares of renewable sources. Note that while this is a limitation of model (1.1') to (8'), it is not a limitation of the state space model class or the general modeling strategy followed in this paper. One could specify a model that instead of emissions uses consumption quantities of fossil and renewable energy carriers as exogenous drivers. Then, observations, forecasts, and scenarios of changes in the consumption quantities of different energy carriers could be employed as input to the model instead of emissions. We have decided not to pursue this avenue since we wanted to engage the time series of the GCB, including emissions. Emissions are in essence linear combinations of the consumed energy carrier quantities, weighted by the physical coefficients that specify how much CO₂ is released by consumption of one unit of the respective carriers (Marland and Rotty, 1984).

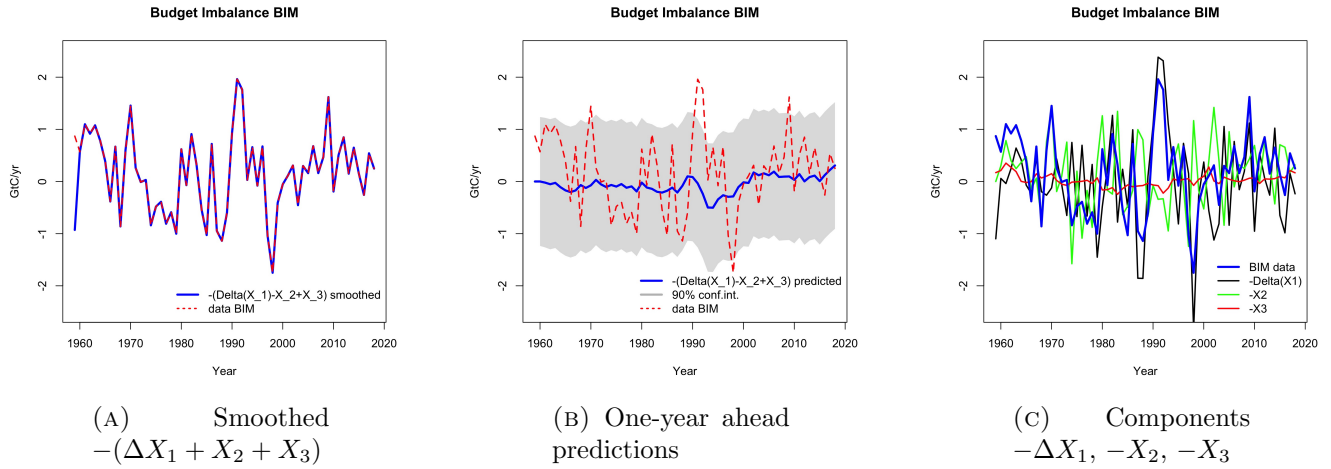
FIGURE 6. Smoothed values for state vector elements of model (1.1') to (8')



Note that because of this definition of emissions, it is not feasible to specify fuel mix variables as explanatory variables on the right-hand side of the E equation, since this will lead to definitional overlap on the left-hand and right-hand side variables. The construction of emissions data is, on the other hand, independent of national accounting and the construction of World GDP data, so that there is no definitional overlap in our specification of the E equation.

6.2. Budget Imbalance. The model facilitates the study of quantities of interest that have been discussed in the literature. For example, Friedlingstein et al. (2019) define and discuss the budget

FIGURE 7. Budget imbalance BIM, smoothed values, one-year ahead predictions, and components



imbalance BIM, which is the residual of the GCB. Model (1.1') to (8') implies $BIM^* = E^* - G_ATM^* - S_LND^* - S_OCN^* = 0$ by way of the equation for G_ATM^* . The corresponding measure of the imbalance in model (1.1') to (8') is

$$\begin{aligned}
 BIM &= E - G_ATM - S_LND - S_OCN, \\
 &= E^* - G_ATM^* - S_LND^* - S_OCN^* - (X_{1,t} - X_{1,t-1}) - X_{2,t} - X_{3,t}, \\
 &= -\Delta X_{1,t} - X_{2,t} - X_{3,t}.
 \end{aligned}$$

Figure 7 panel [A] shows the smoothed values of this (negative) sum together with the data. There is perfect overlap: Since the state processes $E^*-G_ATM^*-S_LND^*-S_OCN^*$ yield zero by definition of the equation for G_ATM^* , all data variation in BIM must be absorbed by the X -processes, which are freely competing for the data variation in the estimation. Note that $X_{4,t}$ in equation (2) for E was found to be insignificant, indicating that there is no stationary variation in emissions that contributes to BIM. From the estimation of the X -processes we can conclude that BIM is stationary, since it is a linear combination of processes that were all tested to be stationary.

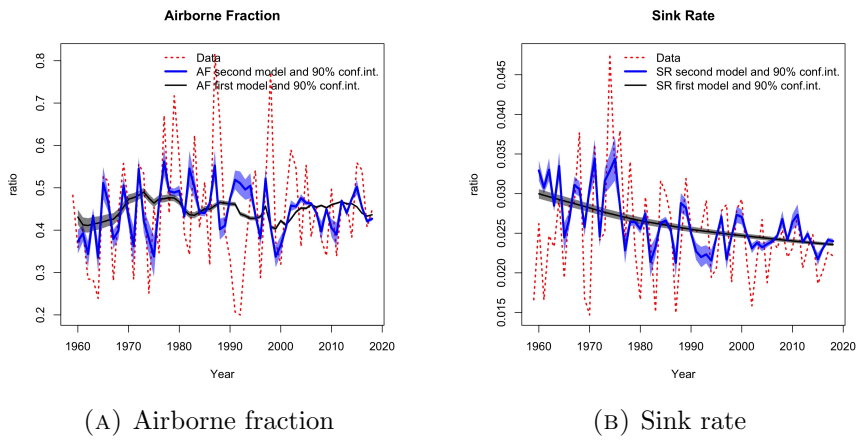
TABLE 8. Empirical covariance matrix of the smoothed values of the components of BIM

	ΔX_1	X_2	X_3
ΔX_1	0.854	-0.358	-0.009
X_2	*	0.449	0.009
X_3	*	*	0.014
Variance decomposition	0.81	0.17	0.02

Figure 7 panel [B] shows the one-year ahead prediction for BIM obtained from the one-year ahead predictions of the X -processes, together with 90% pointwise confidence intervals. Figure 7 panel [C]

shows the individual components $-\Delta X_1$, $-X_2$, and $-X_3$. The panel indicates visually that most of the variation originates in $-\Delta X_1$ and $-X_2$. Table 8 reports the empirical variances and covariances of the smoothed component processes $-\Delta X_1$, $-X_2$, and $-X_3$ of BIM. The variance decomposition confirms the visual inspection of the components: $-\Delta X_1$ (G_ATM) contributes 81% and X_2 (S_LND) 17% to the total variation of BIM. The contribution of X_3 (S_OCN) is smallest at 2%.

FIGURE 8. Airborne fraction and sink rate, smoothed values from second model (1.1') to (8') and from first model (1) to (8), with data for comparison



6.3. Airborne fraction and sink rate. Figure 8 shows the airborne fraction in panel [A] and the sink rate in panel [B]. The airborne fraction

$$AF = \frac{G_ATM}{E}$$

is the part of emissions that remains in the atmosphere. On the sample, this fraction is on average 0.44, but it shows substantial variation in the data. The sink rate

$$SR = \frac{S_LND + S_OCN}{C}$$

is a measure of the capacity of the sinks to absorb atmospheric CO₂. Whether or not the airborne fraction is increasing and/or the sink rate is decreasing has been subject of debate (Canadell et al., 2007a; Raupach et al., 2008; Knorr, 2009; Le Quéré et al., 2009; Gloor et al., 2010; Raupach et al., 2014; Rayner et al., 2015; Ballantyne et al., 2015; Bennedsen et al., 2019b).

Figure 8 shows, however, that by calculating AF^* and SR^* , i.e., the versions of the ratios that have the * -processes in the numerators and denominators of the airborne fraction and the sink rate, we obtain new estimates of these variables that focus on few key relations of the sinks, and thus they show much less variation. Raupach et al. (2014) and Bennedsen et al. (2019b) show that there is no

evidence of an increase in the airborne fraction but that there is evidence of a decline in the sink rate. In Figure 8 this can be seen with the naked eye, in particular for the results from model (1) to (8) that reduces the sinks to linear regressions on concentrations. The figure also shows confidence intervals for both models obtained from simulation smoothing (Durbin and Koopman, 2002). Note that these confidence intervals should not be interpreted such that the data should fall within the boundaries with a certain coverage probability. Rather, their correct interpretation is that if we were given a large number of trajectories sampled from the models, and if we were to extract the smoothed state variables and compute the airborne fraction and the sink rate from these trajectories, the confidence bands will cover these imputed variables 90% of the time.

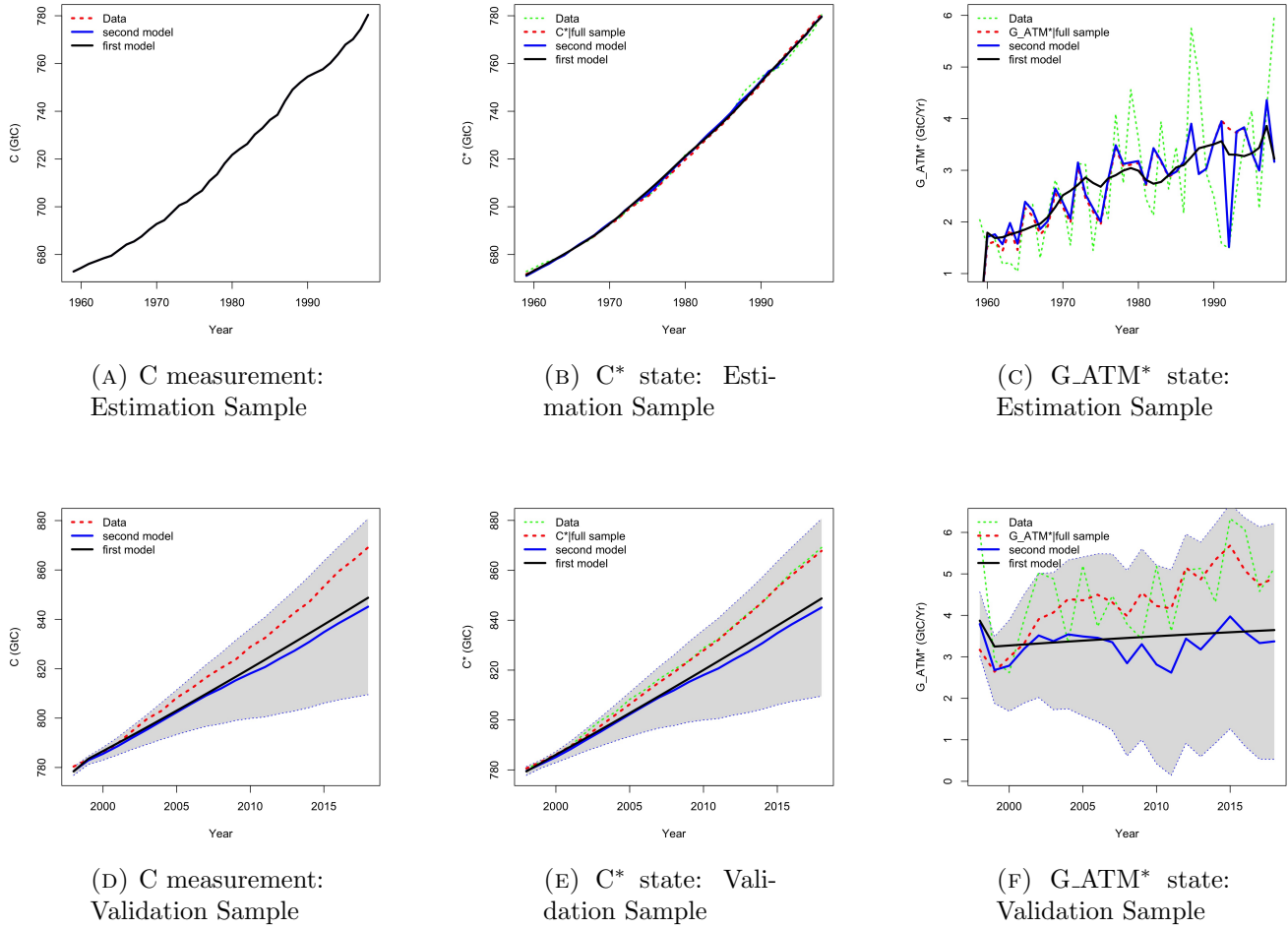
7. VALIDATION, FORECASTS, AND SCENARIO PROJECTIONS

The exogenous drivers of model (1.1') to (8') are World GDP growth and SOI. Given trajectories of these two, all other model objects: emissions E, land sink S_LND, ocean sink S_OCN, growth of atmospheric concentrations G_ATM, and atmospheric concentrations C, are determined up to Gaussian random processes. This facilitates three lines of inquiry: (1) validation, (2) forecasting, and (3) scenario analysis. In validation exercises, the model is estimated on an estimation subsample, and conditional on the data for the exogenous elements, the model is employed to produce implied values for the endogenous variables that can then be compared to the observations from the validation subsample. In forecasting exercises, forecasts of the exogenous drivers are obtained, either by specifying forecast models for them or by getting them from external sources, and they are plugged in to the system to generate forecasts of the endogenous variables. In scenario analyses, usually for long-term projections, artificial trajectories for the exogenous drivers are assumed that are converted, via the model, to corresponding artificial trajectories for the endogenous variables. We discuss these three approaches in the following subsections.

7.1. Validation. We conduct a validation exercise on the last 20 years of the sample, from 1999 to 2018. Model (1.1') to (8') is estimated on the period 1960–1998. Using the estimated parameters and the values of $\Delta \log GDP_{2010,t}$ and SOI_t for the validation sample 1999–2018, the implied values of the system are computed for the 20 years. This results in implied values both for the measurement and for the state variables.

Figure 9 shows the results for C (measurement), C^* (state), and G_ATM^* (state only). The benchmark for the measurement variables are the data series; the benchmark for the states are the states given the full sample, i.e., after estimating the model on the entire sample period 1960–2018

FIGURE 9. Validation Exercise. “First model” refers to Equations (1) to (8), “second model” to Equations (1.1’) to (8’).



and then calculating smoothed values. The benchmark is always shown as red dashed line. In the plots for the states, the data are also shown in green dashed lines. The estimation sample 1960–1998 is shown in separate panels from the validation sample 1999–2018 for each series. The validation is performed on model (1) to (8) (black) as well as on model (1.1’) to (8’) (blue); the pointwise 90% confidence intervals are based on model (1.1’) to (8’).

The plots show that the difference between C and C^* is subtle, since X_1 is small compared to C and C^* . In panel [E], the benchmark of the smoothed state given the full sample and the data lie on top of each other. G_{ATM} exists in our model as state only. Panel [F] shows the validation sample: Both benchmark and data lie within the 90% confidence bands. Black and blue lines show that model (1.1’) to (8’) captures a lot more of the dynamics in the benchmark (and in the data) than model (1) to (8).

FIGURE 10. Validation Exercise. “First model” refers to Equations (1) to (8), “second model” to Equations (1.1’) to (8’).

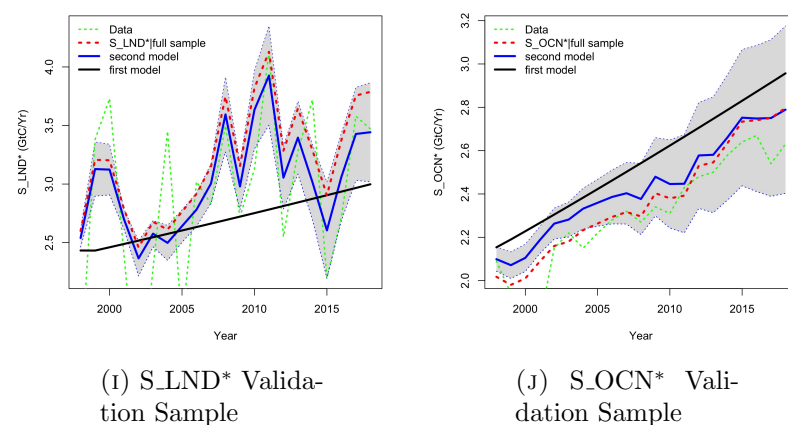
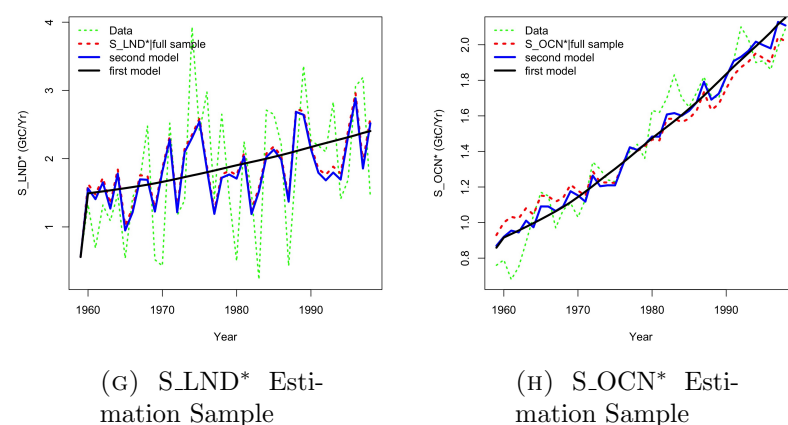
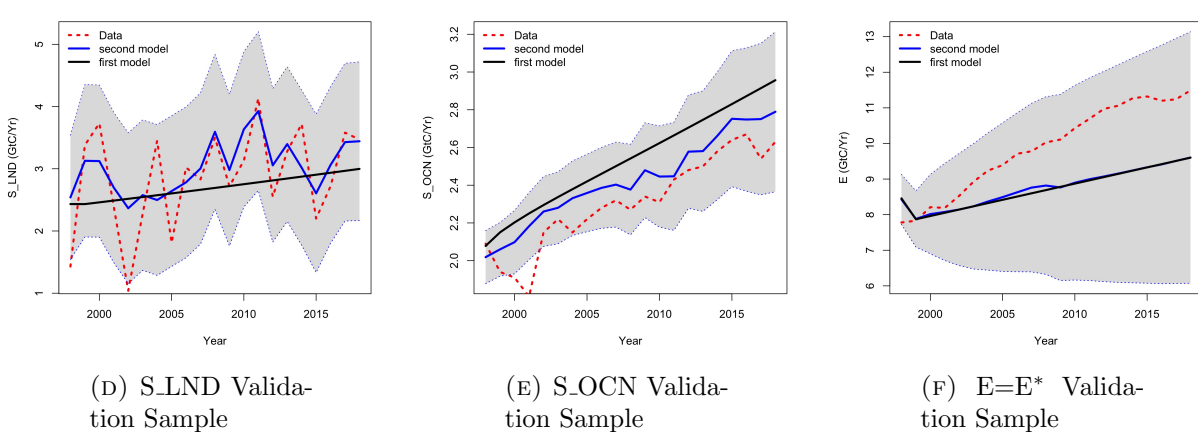
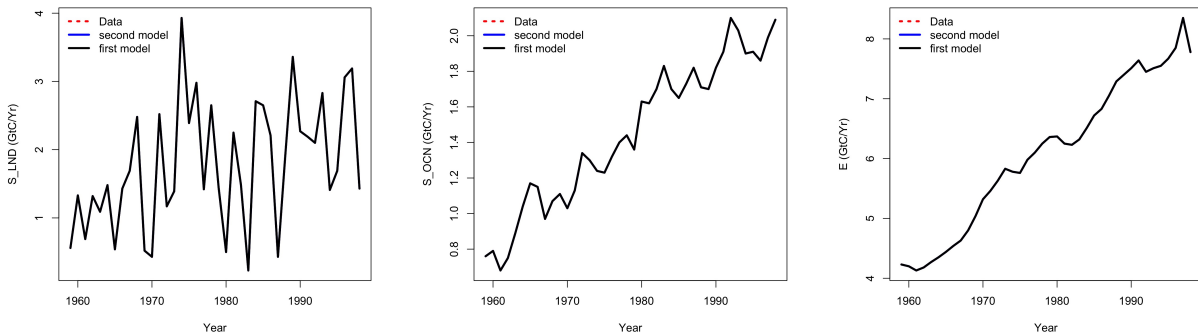


Figure 10 shows the validation results for S_LND, S_OCN, and E. For the sinks, we see marked differences between measurement variables and state variables. For emissions E, there is no difference since the measurement equation specifies equality of measurement and state variable. For the measurement variables on the estimation sample (panels [A] to [C]), we have coincidence of the fitted values from both models with the data, since we model the X -processes in the state equation and do not include independent errors in the measurement equation. (In the notation of Durbin and Koopman (2012), the matrix H is the zero matrix.) On the validation sample, both models perform well in the sense that only few benchmark observations fall outside the confidence bands (panels [D] to [F]). Model (1.1') to (8') captures more of the dynamics in the data than model (1) to (8), and the fitted values lie closer to the sink data. For E, there is little difference in the fitted values from either model.

For the sink states, there is a marked difference between models (1.1') to (8') and (1) to (8) on the estimation sample (panels [G] and [H]), with the extended specification capturing the data substantially better. This pattern extends into the validation sample (panels [I] and [J]), where model (1.1') to (8') outperforms the simpler model both in terms of proximity to the benchmark as well as proximity to the data.

In summary, the validation exercise shows that model (1.1') to (8') describes the GCB data well. Even on a validation sample of the size of a third of the entire sample period, it can generate implied values and confidence bands from parameters estimated on the first 40 years and from data on $\Delta \log GDP$ and on SOI such that the data and the smoothed states obtained from the full sample lie reasonably within confidence bounds.

7.2. Forecasts. Given the data sample period from 1959 to 2018, we forecast/nowcast models (1.1') to (8') and (1) to (8) for the periods 2019 to 2021. This necessitates forecasting World GDP growth and the Southern Oscillation Index (SOI).

For World GDP growth, we resort to the forecasts regularly provided and updated by the International Monetary Fund (IMF) and the World Bank (WB). Table 9 reports nowcasts for 2019 reported in IMF (July 2019) and World Bank (June 2019) and nowcasts and forecasts for 2020 and 2021 reported in IMF (June 2020) and World Bank (June 2020a).

We forecast the monthly Southern Oscillation Index obtained from Climatic Research Unit (2020) and Ropelewski and Jones (1987) with a basic structural time series model that consists of a monthly seasonal component, a second-order stochastic cycle whose period is estimated close to 4 years, and a first-order autoregressive cycle component, compare (Durbin and Koopman, 2012, Section 3.2) and

TABLE 9. Forecasts of World GDP growth provided by International Monetary Fund and World Bank (in percent). Nowcasts for 2019 are from IMF (July 2019) and World Bank (June 2019). Nowcasts and forecasts for 2020 and 2021 are from IMF (June 2020) and World Bank (June 2020a). Data are from World Bank (2020b).

	2019	2020	2021
IMF	3.2%	-4.9%	5.4%
World Bank	2.6%	-5.2%	4.2%
Data	2.4%	N/A	N/A

Azevedo et al. (2006). We describe details of the forecast model in Appendix B. For 2019, we obtain an annual value of the SOI of -0.808 from data; for 2020 and 2021, we obtain forecast values of SOI of -0.0453 and 0.1926, respectively; see the explanations in the appendix.

FIGURE 11. Forecasts of C , G_{ATM} , E , S_{LND} , and S_{OCN} from Model 2 (equations (1.1') to (8'), blue) and Model 1 (equations (1) to (8), black) with 90% pointwise confidence intervals. Model 2 employs forecasts of SOI generated from the model described in Appendix B and forecasts of World GDP growth from the IMF. Forecasts obtained with World GDP growth forecasts from the World Bank are visually identical, compare Table 10.

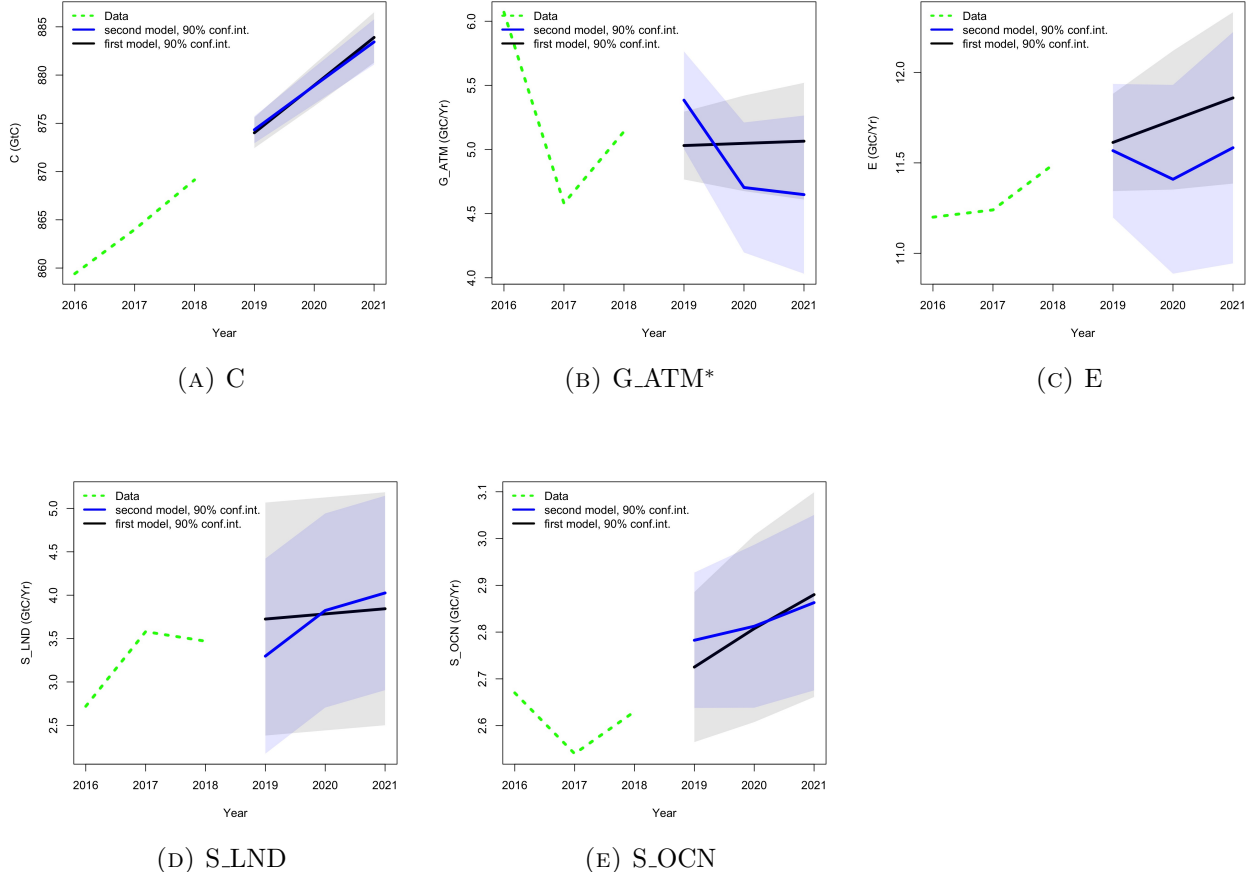


Table 10 and Figure 11 show the forecasts together with estimates of the forecast uncertainty (forecast standard errors in Table 10 and 90% pointwise confidence bands in Figure 11). On the

TABLE 10. Forecasts of C , G_{ATM} , E , S_{LND} , and S_{OCN} from Model 2 (equations (1.1') to (8')) and Model 1 (equations (1) to (8)), given forecasts of World GDP growth and SOI. Forecast standard errors in parentheses.

	2019		2020		2021				
	Model 2		Model 2		Model 2				
	IMF	WB	Model 1	IMF	WB	Model 1			
C (GtC)	874.33 (0.852)	874.33 (0.852)	874.02 (0.968)	878.90 (1.159)	878.89 (1.159)	878.94 (1.323)	883.43 (1.430)	883.38 (1.430)	883.90 (1.592)
G_{ATM} (GtC/Yr)	5.385 (0.232)	5.385 (0.232)	5.031 (0.161)	4.704 (0.309)	4.694 (0.309)	5.048 (0.227)	4.648 (0.376)	4.601 (0.376)	5.064 (0.277)
E (GtC/Yr)	11.568 (0.225)	11.568 (0.225)	11.613 (0.164)	11.409 (0.318)	11.400 (0.318)	11.736 (0.234)	11.584 (0.390)	11.535 (0.390)	11.859 (0.289)
S_{LND} (GtC/Yr)	3.298 (0.686)	3.298 (0.686)	3.725 (0.819)	3.824 (0.682)	3.824 (0.682)	3.784 (0.819)	4.026 (0.683)	4.025 (0.683)	3.844 (0.819)
S_{OCN} (GtC/Yr)	2.783 (0.088)	2.783 (0.088)	2.725 (0.098)	2.813 (0.106)	2.812 (0.106)	2.807 (0.122)	2.863 (0.114)	2.862 (0.114)	2.880 (0.133)

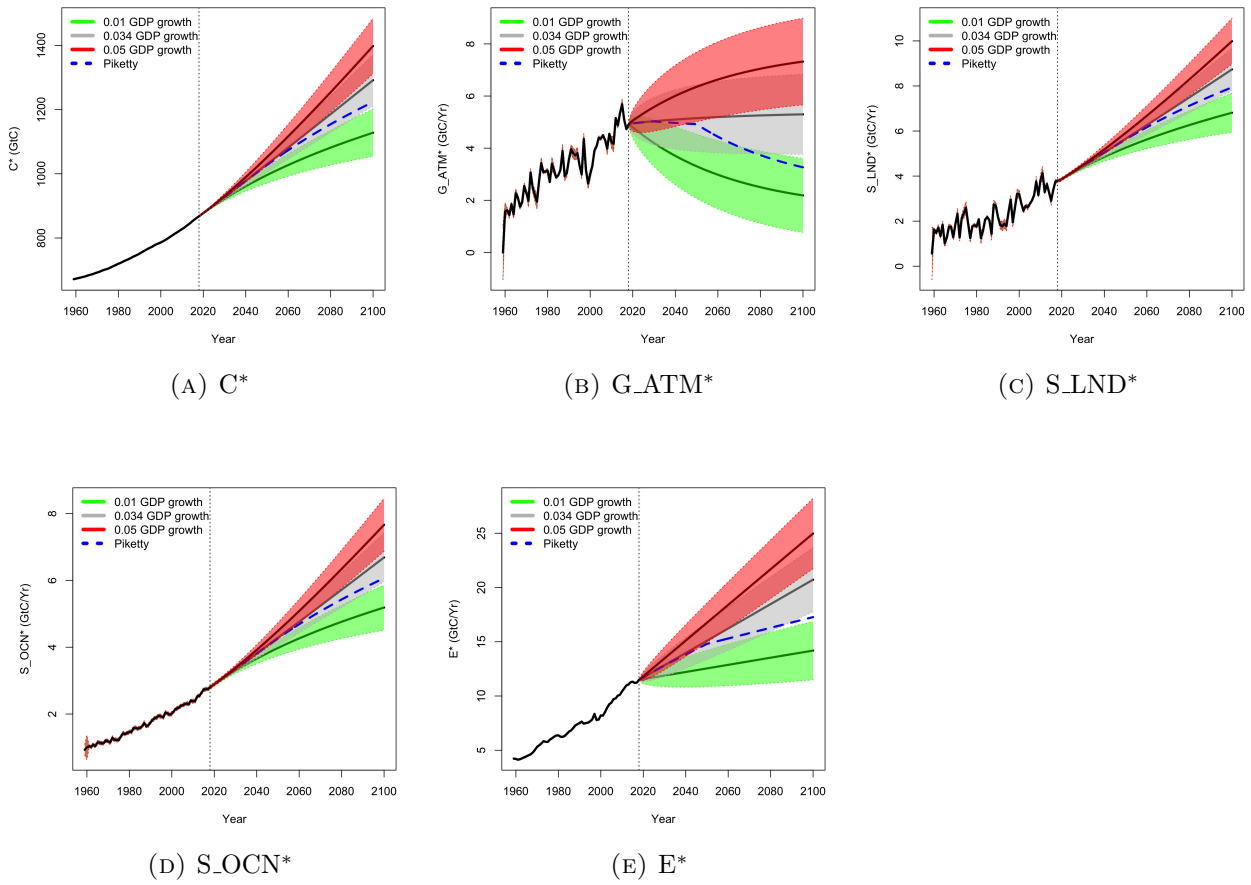
three points of the forecast sample, the forecasts from models (1) to (8) and (1.1') to (8') are broadly comparable, in particular as regards atmospheric concentrations C . There are, however, some differences in G_{ATM}^* , E , S_{LND} , and S_{OCN} that reflect the ability of model (1.1') to (8') to reflect the forecasts of World GDP and SOI. Both forecasts reflect substantial changes: World GDP in 2020 is expected to decrease by about 5%, a historically large negative change due to the COVID-19 pandemic, followed by a rebound that is forecast to be of about the same size in 2021. The SOI is predicted to switch from an El-Niño period (negative numbers) to a La-Niña period (positive numbers) between 2020 and 2021, although the difference in the forecasts between the two consecutive years is not unusually large. These dynamics are reflected in the forecasts of G_{ATM}^* , E , S_{LND} , and S_{OCN} : Emissions E are forecast from model (1.1') to (8') to decrease in 2020 and to increase again in 2021 to about the level of 2019. G_{ATM}^* is also forecast to decrease as a consequence of this, followed by a largely lateral movement between 2020 and 2021. The sink processes are forecast to react moderately to these changes in the exogenous variables. Note that the consequences of these changes for the forecasts of C are negligible. Model (1) to (8), which does not take any of this information into account and simply extrapolates from the 1959–2018 dynamics, arrives at a very similar forecast for atmospheric concentrations.

7.3. Scenario analysis. We consider four scenarios for world GDP growth using model (1.1') to (8'). Scenario 1 considers a constant annual growth rate between 2019 and 2100 of 0.01, Scenario 2 considers a constant annual growth rate equal to the historical mean 0.034 measured on the 1959–2018 period, and Scenario 3 considers a constant annual growth rate equal to 0.05. Scenario 4, labeled “Piketty”, is proposed in (Piketty, 2014, p. 101) and considers an annual growth rate of 0.034 until 2030, 0.03 from 2031 to 2050, and 0.015 from 2051 to 2100. The rationale for the decreasing

growth rates is essentially the increasing dominance of services in the composition of world output as economies mature, see the discussion in Piketty (2014). In all scenarios, SOI is set to zero, i.e., we are not using scenarios for ENSO. Thus, GDP growth is the only exogenous variable of the system of equations of model (1.1') to (8').

The following graphs show the paths of the states C^* , G_{ATM}^* , S_{LND}^* , S_{OCN}^* and E^* together with pointwise 90% confidence bands for Scenarios 1 to 3 based on smoothed states and smoothed state variances.

FIGURE 12. Scenario analysis



8. CONCLUSIONS AND DIRECTIONS FOR FURTHER RESEARCH

In this paper, we proposed a statistical system model for the global carbon budget, consisting of the time series objects atmospheric CO₂ concentrations, anthropogenic CO₂ emissions, land and ocean CO₂ uptake (sinks). The keystone of the model is the budget equation that the fraction of emissions that is not absorbed by the terrestrial biosphere and the ocean constitutes an annual flow to the stock of atmospheric concentrations. We discussed the central assumptions of random walk with drift dynamics for anthropogenic emissions and linear dependence of sinks on atmospheric concentrations.

The model equations then allow for a closed-form solution for atmospheric concentrations that reveal stochastic integration of order one with a second near unit root. This shows that the deterministic trend in concentrations is linear, but will on finite samples appear quadratic due to the second near unit root. We also discussed that the second root moves closer to unity with increasing atmospheric concentrations.

We showed in Monte Carlo simulations that estimating the model by maximum likelihood with the help of the Kalman filter has good properties even on finite samples. We estimated the model on the global carbon budget data set provided by the Global Carbon Project and discussed the residual diagnostics, parameter estimates, and projections of the states. We then presented a decomposition of the variation in the budget imbalance into contributions from concentrations, land sink, and ocean sink. We discussed the airborne fraction and sink rate implied by our model.

We presented a number of out-of-sample exercises and pseudo-out-of-sample exercises. First, we estimated the model on the first 40 years of data and validated it on the last 20 years of data. Second, we used the model, together with forecasts of World-GDP and of SOI, to forecast anthropogenic emissions, atmospheric concentrations, land sink, and ocean sink for three years into the future. Finally, employing different scenarios for future GDP growth, we projected possible future paths for the four time series.

There are several directions in which we plan to extend the model in the future. Given the model's structure, it is conceptually straightforward to not just include the averages of the ensemble models for S_LND and S_OCN but the individual ensemble members themselves. The structure is also conducive for increasing the resolution on the macroeconomic sphere, for example by replacing World-GDP in emissions by factors obtained from large macroeconomic data sets. The mechanics of the global carbon cycle can be extended to include, for example, elements of the widely used MAGICC model. The model structure can be extended by energy balance modules to provide a modeling connection to global temperatures. Finally, this paper showed that the system relations between the variables of the global carbon budget can also be understood within the framework of cointegration, and we are working on this perspective.

APPENDIX A. SYSTEM MATRICES

Motivated by the findings in Section 4, which are summarily listed in the beginning of Section 5, we specify the residual processes as follows.

$$(20) \quad X_{1,t+1} = \phi_1 X_{1,t} + \eta_{1,t+1},$$

$$(21) \quad X_{2,t+1} = \eta_{2,t+1},$$

$$(22) \quad X_{3,t+1} = \phi_3 X_{3,t} + \eta_{3,t+1},$$

$$(23) \quad X_{4,t+1} = \eta_{4,t+1},$$

where $\phi_{1,3} \in (-1, 1)$. Defining the measurement vector as $y_t = (C_t, E_t, S_LND_t, S_OCN_t)'$ and the state vector as $\alpha_t = (C_t^*, G_ATM_t^*, S_LND_t^*, S_OCN_t^*, X_{1,t}, X_{2,t}, X_{3,t}, X_{4,t}, E_t^*)'$, the model can be represented as

$$(24) \quad \begin{aligned} y_t &= Z\alpha_t, \\ B\alpha_{t+1} &= \tilde{c} + \tilde{T}\alpha_t + \tilde{\eta}_t, \end{aligned}$$

where the matrix B contains the contemporary relations: G_ATM depending on concurrent E, S_LND, and S_OCN, the sinks depending on concurrent C.

Pre-multiplying the state equation with B^{-1} transforms model (24) to standard state space form:

$$(25) \quad \begin{aligned} y_t &= Z\alpha_t, \\ \alpha_{t+1} &= c + T\alpha_t + \eta_t. \end{aligned}$$

Explicitly, (25) is given by the measurement equation

$$\begin{bmatrix} C_t \\ E_t \\ S_LND_t \\ S_OCN_t \end{bmatrix} = \begin{bmatrix} 1 & 0 & 0 & 0 & 1 & 0 & 0 & 0 & 0 \\ 0 & 0 & 0 & 0 & 0 & 0 & 0 & 1 & 1 \\ 0 & 0 & 1 & 0 & 0 & 1 & 0 & 0 & 1 \\ 0 & 0 & 0 & 1 & 0 & 0 & 1 & 0 & 1 \end{bmatrix} \begin{bmatrix} C_t^* \\ G_ATM_t^* \\ S_LND_t^* \\ S_OCN_t^* \\ X_{1,t} \\ X_{2,t} \\ X_{3,t} \\ X_{4,t} \\ E_t^* \end{bmatrix}.$$

The state equation is

$$\begin{bmatrix} 1 & -1 & 0 & 0 & 0 & 0 & 0 & 0 & 0 \\ 0 & 1 & 1 & 1 & 0 & 0 & 0 & 0 & -1 \\ -\frac{\beta_1}{C_0} & 0 & 1 & 0 & 0 & 0 & 0 & 0 & 0 \\ -\frac{\beta_2}{C_0} & 0 & 0 & 1 & 0 & 0 & 0 & 0 & 0 \\ 0 & 0 & 0 & 0 & 1 & 0 & 0 & 0 & 0 \\ 0 & 0 & 0 & 0 & 0 & 1 & 0 & 0 & 0 \\ 0 & 0 & 0 & 0 & 0 & 0 & 1 & 0 & 0 \\ 0 & 0 & 0 & 0 & 0 & 0 & 0 & 1 & 0 \\ 0 & 0 & 0 & 0 & 0 & 0 & 0 & 0 & 1 \end{bmatrix} \begin{bmatrix} C_{t+1}^* \\ G_ATM_{t+1}^* \\ S_LND_{t+1}^* \\ S_OCN_{t+1}^* \\ X_{1,t+1} \\ X_{2,t+1} \\ X_{3,t+1} \\ X_{4,t+1} \\ E_{t+1}^* \end{bmatrix} = \begin{bmatrix} 1 & 0 & 0 & 0 & 0 & 0 & 0 & 0 & 0 \\ 0 & 0 & 0 & 0 & 0 & 0 & 0 & 0 & 0 \\ 0 & 0 & 0 & 0 & 0 & 0 & 0 & 0 & 0 \\ 0 & 0 & 0 & 0 & 0 & 0 & 0 & 0 & 0 \\ 0 & 0 & 0 & 0 & 0 & \phi_1 & 0 & 0 & 0 \\ 0 & 0 & 0 & 0 & 0 & 0 & 0 & 0 & 0 \\ 0 & 0 & 0 & 0 & 0 & 0 & 0 & \phi_3 & 0 \\ 0 & 0 & 0 & 0 & 0 & 0 & 0 & 0 & 0 \\ 0 & 0 & 0 & 0 & 0 & 0 & 0 & 0 & 1 \end{bmatrix} \begin{bmatrix} C_t^* \\ G_ATM_t^* \\ S_LND_t^* \\ S_OCN_t^* \\ X_{1,t} \\ X_{2,t} \\ X_{3,t} \\ X_{4,t} \\ E_t^* \end{bmatrix}$$

$$+ \begin{bmatrix} 0 \\ 0 \\ c_1 \\ c_2 \\ 0 \\ 0 \\ 0 \\ 0 \\ d \end{bmatrix} + \begin{bmatrix} 0 \\ 0 \\ \eta_{1,t} \\ \eta_{2,t} \\ \eta_{3,t} \\ \eta_{4,t} \\ \eta_{5,t} \end{bmatrix},$$

where $\eta_{5,t} = \eta_t^E$. It holds that

$$\begin{bmatrix} 1 & -1 & 0 & 0 & 0 & 0 & 0 & 0 & 0 \\ 0 & 1 & 1 & 1 & 0 & 0 & 0 & 0 & -1 \\ -\frac{\beta_1}{C_0} & 0 & 1 & 0 & 0 & 0 & 0 & 0 & 0 \\ -\frac{\beta_2}{C_0} & 0 & 0 & 1 & 0 & 0 & 0 & 0 & 0 \\ 0 & 0 & 0 & 0 & 1 & 0 & 0 & 0 & 0 \\ 0 & 0 & 0 & 0 & 0 & 1 & 0 & 0 & 0 \\ 0 & 0 & 0 & 0 & 0 & 0 & 1 & 0 & 0 \\ 0 & 0 & 0 & 0 & 0 & 0 & 0 & 1 & 0 \end{bmatrix}^{-1} = \begin{bmatrix} \frac{1}{c} & \frac{1}{c} & \frac{-1}{c} & \frac{-1}{c} & 0 & 0 & 0 & 0 & \frac{1}{c} \\ \frac{-(\beta_1^* + \beta_2^*)}{c} & \frac{1}{c} & \frac{-1}{c} & \frac{-1}{c} & 0 & 0 & 0 & 0 & \frac{1}{c} \\ \frac{\beta_1^*}{c} & \frac{\beta_1^*}{c} & \frac{1+\beta_2^*}{c} & \frac{-\beta_1^*}{c} & 0 & 0 & 0 & 0 & \frac{\beta_1^*}{c} \\ \frac{\beta_2^*}{c} & \frac{\beta_2^*}{c} & \frac{-\beta_2^*}{c} & \frac{1+\beta_1^*}{c} & 0 & 0 & 0 & 0 & \frac{\beta_2^*}{c} \\ 0 & 0 & 0 & 0 & 1 & 0 & 0 & 0 & 0 \\ 0 & 0 & 0 & 0 & 0 & 1 & 0 & 0 & 0 \\ 0 & 0 & 0 & 0 & 0 & 0 & 1 & 0 & 0 \\ 0 & 0 & 0 & 0 & 0 & 0 & 0 & 1 & 0 \\ 0 & 0 & 0 & 0 & 0 & 0 & 0 & 0 & 1 \end{bmatrix},$$

where

$$\beta_1^* = \frac{\beta_1}{C_0}, \quad \beta_2^* = \frac{\beta_2}{C_0}, \quad c = 1 + \beta_1^* + \beta_2^*.$$

Then,

and

$$\left[\begin{array}{ccccccccc} \frac{1}{c} & \frac{1}{c} & \frac{-1}{c} & \frac{-1}{c} & 0 & 0 & 0 & 0 & \frac{1}{c} \\ \frac{-(\beta_1^* + \beta_2^*)}{c} & \frac{1}{c} & \frac{-1}{c} & \frac{-1}{c} & 0 & 0 & 0 & 0 & \frac{1}{c} \\ \frac{\beta_1^*}{c} & \frac{\beta_1^*}{c} & \frac{1+\beta_2^*}{c} & \frac{-\beta_1^*}{c} & 0 & 0 & 0 & 0 & \frac{\beta_1^*}{c} \\ \frac{\beta_2^*}{c} & \frac{\beta_2^*}{c} & \frac{-\beta_2^*}{c} & \frac{1+\beta_1^*}{c} & 0 & 0 & 0 & 0 & \frac{\beta_2^*}{c} \\ 0 & 0 & 0 & 0 & 1 & 0 & 0 & 0 & 0 \\ 0 & 0 & 0 & 0 & 0 & 1 & 0 & 0 & 0 \\ 0 & 0 & 0 & 0 & 0 & 0 & 1 & 0 & 0 \\ 0 & 0 & 0 & 0 & 0 & 0 & 0 & 1 & 0 \\ 0 & 0 & 0 & 0 & 0 & 0 & 0 & 0 & 1 \end{array} \right] \left[\begin{array}{c} 0 \\ 0 \\ 0 \\ 0 \\ \eta_{1,t} \\ \eta_{2,t} \\ \eta_{3,t} \\ \eta_{4,t} \\ \eta_{5,t} \end{array} \right] = \left[\begin{array}{c} \frac{1}{c} \eta_{5,t} \\ \frac{1}{c} \eta_{5,t} \\ \frac{\beta_1^*}{c} \eta_{5,t} \\ \frac{\beta_2^*}{c} \eta_{5,t} \\ \eta_{1,t} \\ \eta_{2,t} \\ \eta_{3,t} \\ \eta_{4,t} \\ \eta_{5,t} \end{array} \right].$$

To obtain a representation as $R\eta_t$, this can be written as

$$\begin{bmatrix} \frac{1}{c}\eta_{5,t} \\ \frac{1}{c}\eta_{5,t} \\ \frac{\beta_1^*}{c}\eta_{5,t} \\ \frac{\beta_2^*}{c}\eta_{5,t} \\ \eta_{1,t} \\ \eta_{2,t} \\ \eta_{3,t} \\ \eta_{4,t} \\ \eta_{5,t} \end{bmatrix} = \begin{bmatrix} 0 & 0 & 0 & 0 & 0 & 0 & 0 & 0 & \frac{1}{c} \\ 0 & 0 & 0 & 0 & 0 & 0 & 0 & 0 & \frac{1}{c} \\ 0 & 0 & 0 & 0 & 0 & 0 & 0 & 0 & \frac{\beta_1^*}{c} \\ 0 & 0 & 0 & 0 & 0 & 0 & 0 & 0 & \frac{\beta_2^*}{c} \\ 0 & 0 & 0 & 0 & 1 & 0 & 0 & 0 & 0 \\ 0 & 0 & 0 & 0 & 0 & 1 & 0 & 0 & 0 \\ 0 & 0 & 0 & 0 & 0 & 0 & 1 & 0 & 0 \\ 0 & 0 & 0 & 0 & 0 & 0 & 0 & 1 & 0 \\ 0 & 0 & 0 & 0 & 0 & 0 & 0 & 0 & 1 \end{bmatrix} \begin{bmatrix} 0 \\ 0 \\ 0 \\ 0 \\ \eta_{1,t} \\ \eta_{2,t} \\ \eta_{3,t} \\ \eta_{4,t} \\ \eta_{5,t} \end{bmatrix}.$$

The covariance matrix Q of the errors η_t in the state equation is given by zeros except the entries in rows and columns 5 to 9, which are

$$Q[5 : 8, 5 : 8] = \begin{bmatrix} \sigma_{\eta_1}^2 & r_{12}\sigma_{\eta_1}\sigma_{\eta_2} & r_{13}\sigma_{\eta_1}\sigma_{\eta_3} & 0 & 0 \\ r_{12}\sigma_{\eta_1}\sigma_{\eta_2} & \sigma_{\eta_2}^2 & 0 & 0 & 0 \\ r_{13}\sigma_{\eta_1}\sigma_{\eta_3} & 0 & \sigma_{\eta_3}^2 & 0 & 0 \\ 0 & 0 & 0 & \sigma_{\eta_4}^2 & 0 \\ 0 & 0 & 0 & 0 & \sigma_{\eta_5}^2 \end{bmatrix}.$$

APPENDIX B. FORECAST MODEL FOR SOUTHERN OSCILLATION INDEX

The forecast model for monthly data on the Southern Oscillation Index (SOI) covering the period Jan-1866 to Jul-2020, obtained from Climatic Research Unit (2020) and Ropelewski and Jones (1987), is a basic structural time series model as outlined in (Durbin and Koopman, 2012, Section 3.2). The model is

$$(26) \quad SOI_t = \psi_t + \sum_{j=1}^6 \gamma_{j,t} + \varepsilon_t,$$

$$\varepsilon_t = \phi\varepsilon_{t-1} + \eta_t,$$

where ψ_t is a cycle component defined below, $\eta_t \sim N(0, \sigma_\eta^2)$, and $|\phi| < 1$. The monthly seasonal component is defined as

$$(27) \quad \gamma_{j,t} = \tilde{\gamma}_j \cos \lambda_j t + \tilde{\gamma}_j^* \sin \lambda_j t,$$

$$(28) \quad \gamma_{j,t} = -\tilde{\gamma}_j \sin \lambda_j t + \tilde{\gamma}_j^* \cos \lambda_j t,$$

and

$$\lambda_j = \frac{2\pi j}{12}.$$

A chi-square test for seasonality strongly rejects the null of no seasonality (29.205, with p -value 0.0021). Specifying a stochastic version of the seasonal component, where equation (27) contains a random error variable, resulted in an estimated variance indistinguishable from zero, and thus the deterministic form displayed above was adopted here.

The cycle component ψ_t is defined as $\psi_t = \psi_t^{(2)}$, where

$$\begin{bmatrix} \psi_{t+1}^{(j)} \\ \psi_{t+1}^{*(j)} \end{bmatrix} = \begin{bmatrix} \cos \lambda & \sin \lambda \\ -\sin \lambda & \cos \lambda \end{bmatrix} \begin{bmatrix} \psi_t^{(j)} \\ \psi_t^{*(j)} \end{bmatrix} + \begin{bmatrix} \psi_t^{(j-1)} \\ \psi_t^{*(j-1)} \end{bmatrix}, j = 1, 2,$$

with

$$\psi_t^{(0)} = \kappa_t \sim N(0, \sigma_\kappa^2) \quad \text{and} \quad \psi_t^{*(0)} = \kappa_t^* \sim N(0, \sigma_\kappa^2).$$

This is a second-order stochastic trigonometric cycle component with period $2\pi/\lambda$ (Azevedo et al., 2006). The frequency is estimated as $\hat{\lambda} = 0.1286$, translating to an estimated period of 48.9 months or about 4 years.

Including a local linear form of a trend and intercept term in (26) in addition to the AR-error and the seasonal structure,

$$\mu_t = \mu_{t-1} + \nu_{t-1} + \xi_{t-1}, \quad \xi_t \sim N(0, \sigma_\xi^2),$$

$$\nu_t = \nu_{t-1} + \zeta_{t-1}, \quad \zeta_t \sim N(0, \sigma_\zeta^2),$$

resulted in estimated variances σ_ξ^2 and σ_ζ^2 indistinguishable from zero, and thus the deterministic form $\mu + \nu t$ was tested next. The estimation resulted in insignificant coefficients μ and ν , consistent with the cyclical nature of El-Niño and La-Niña phases, and so the specification (26) with cycle, season, and AR(1) error was chosen.

Figure 13 shows the SOI data in the upper left panel, the smoothed cycle component $E(\hat{\psi}_t | Y_T)$ in the upper right panel, the smoothed seasonal component $E(\sum_{j=1}^6 \hat{\gamma}_{j,t} | Y_T)$ in the middle left panel,

the smoothed AR(1) component $E(\hat{\varepsilon}_t | Y_T)$ in the middle right panel, and the smoothed residual $E(\hat{\eta}_t | Y_T)$ in the lower left panel. Here, Y_T is the data on the entire sample.

FIGURE 13. Fitted forecast model for SOI

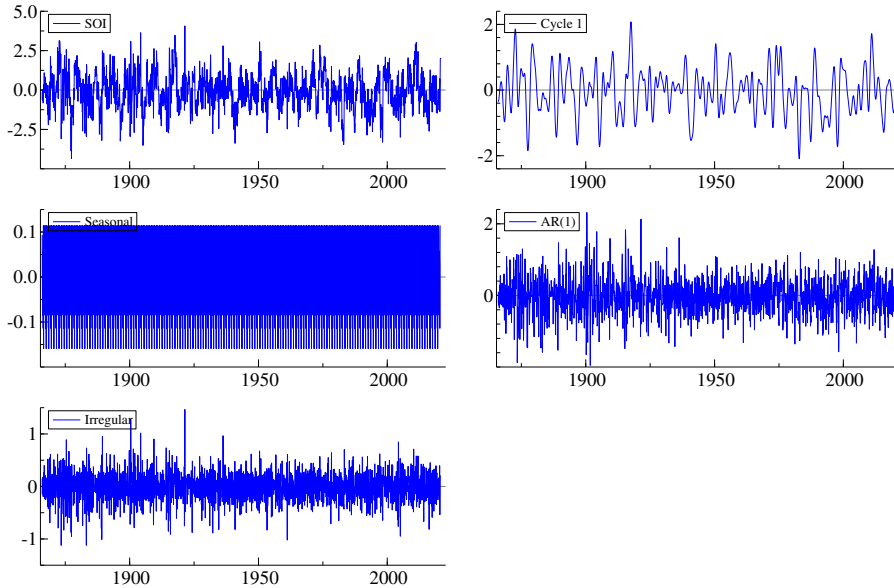
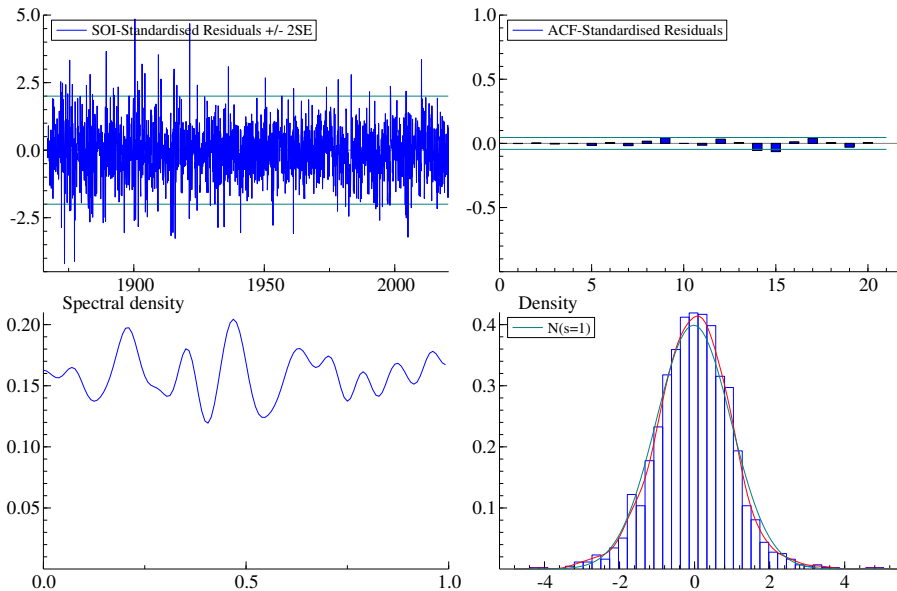


Figure 14 shows the standardized residuals from the one-step-ahead prediction in the upper left panel, the estimated sample autocorrelation function of the residuals in the upper right panel, a smoothed periodogram of the residuals in the bottom left and a histogram of the residuals in the bottom right panel.

FIGURE 14. Residuals from forecast model for SOI



The Durbin-Watson statistic of the residuals is 2.00; the R^2 of the regression is 0.26. The Ljung-Box statistics for the first 12 lags of residuals are not significant at the 95% confidence level, despite the high number of observations ($T = 1855$).

The estimated parameters of the forecast model are reported in Table 11. The forecast values for Aug-2020 through Dec-2021 are shown in Table 12. These forecast values were used to produce the annual forecasts of SOI used in the forecast of the global carbon budget system in Model 2, equations (1.1') to (8'), displayed in Figures 11 and Table 10. These annual forecasts are the averages of the monthly values and are -0.045 for 2020 (consisting of data through Jul 20 and of forecasts from Aug to Dec 20) and 0.193 for 2021.

TABLE 11. Estimated parameters for model (26).

	ϕ	λ	σ_k^2	γ_1	γ_1^*	γ_2	γ_2^*	γ_3	γ_3^*	γ_4	γ_4^*	γ_5	γ_5^*	γ_6
Estimate	0.39	0.129	0.01	-0.03	1e-4	0.02	-0.03	-0.03	0.04	0.05	-0.02	0.07	-0.03	0.03
std.err.				0.04	0.04	0.03	0.03	0.02	0.02	0.02	0.02	0.02	0.02	0.02

FIGURE 15. Forecasts for SOI

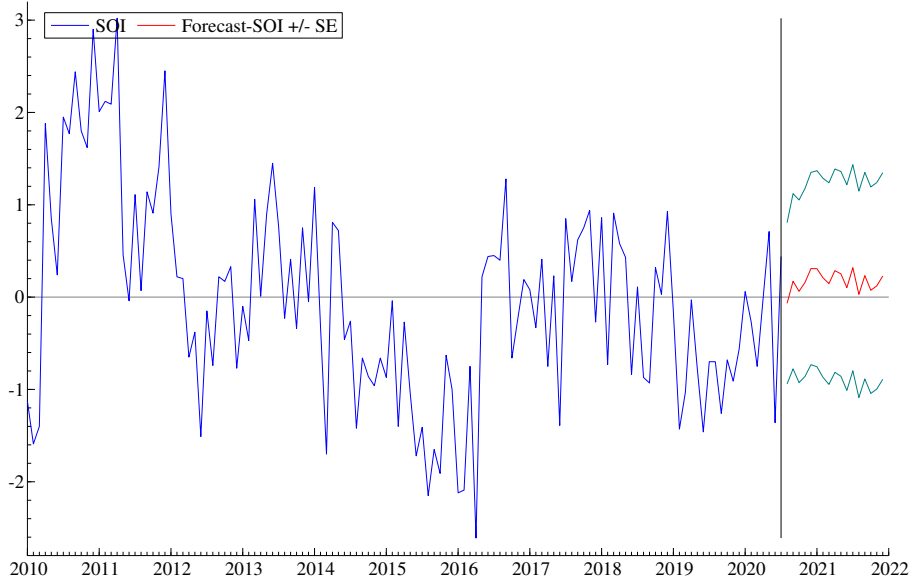


TABLE 12. Forecasts of SOI Aug-2020 through Dec-2021.

Aug 2020	-0.067
Sep 2020	0.172
Oct 2020	0.063
Nov 2020	0.159
Dec 2020	0.309
Jan 2021	0.307
Feb 2021	0.209
Mar 2021	0.146
Apr 2021	0.287
May 2021	0.252
Jun 2021	0.103
Jul 2021	0.319
Aug 2021	0.030
Sep 2021	0.233
Oct 2021	0.075
Nov 2021	0.122
Dec 2021	0.229

REFERENCES

- Adcroft, A., W. Anderson, V. Balaji, C. Blanton, M. Bushuk, C.O. Dufour, J.P. Dunne, S.M. Griffies, R. Hallberg, M.J. Harrison et al.**, “The GFDL global ocean and sea ice model OM4. 0: Model description and simulation features,” *Journal of Advances in Modeling Earth Systems*, 2019, 11 (10), 3167–3211.
- Aumont, O., C. Éthé, A. Tagliabue, L. Bopp, and M. Gehlen**, “PISCES-v2: an ocean biogeochemical model for carbon and ecosystem studies,” *Geoscientific Model Development Discussions*, 2015, 8 (2).
- Azevedo, J.V., S.J. Koopman, and A. Rua**, “Tracking the Business Cycle of the Euro Area,” *Journal of Business and Economic Statistics*, 2006, 24, 278–290.
- Bacastow, R. and C. D. Keeling**, “Atmospheric Carbon Dioxide and radiocarbon in the natural cycle: II. Changes from A. D. 1700 to 2070 as deduced from a geochemical model,” in “Carbon and the biosphere conference proceedings; Upton, New York, USA,” Brookhaven Symposia in Biology, 1973, pp. 86–135.
- Ballantyne, A. P., R. Andres, R. Houghton, B. D. Stocker, R. Wanninkhof, W. Anderegg, L. A. Cooper, M. DeGrandpre, P. P. Tans, J. B. Miller, C. Alden, and J. W. C. White**, “Audit of the global carbon budget: estimate errors and their impact on uptake uncertainty,” *Biogeosciences*, 2015, 12 (8), 2565–2584.
- Barsky, R.B. and L. Kilian**, “Oil and the Macroeconomy since the 1970s,” *Journal of Economic Perspectives*, 2004, 18 (4), 115–134.
- Bennedsen, M., E. Hillebrand, and S.J. Koopman**, “Modeling, Forecasting, and Nowcasting U.S. CO₂ Emissions Using Many Macroeconomic Predictors,” Technical Report, CREATES Working Paper 2019-21 2019a.
- _____, _____, and _____, “Trend analysis of the airborne fraction and sink rate of anthropogenically released CO₂,” *Biogeosciences*, 2019b, 16 (18), 3651–3663.
- Berthet, S., R. Séférion, C. Bricaud, M. Chevallier, A. Voldoire, and C. Ethé**, “Evaluation of an online grid-coarsening algorithm in a global eddy-admitting ocean biogeochemical model,” *Journal of Advances in Modeling Earth Systems*, 2019, 11 (6), 1759–1783.
- Blanco, G., R. Gerlagh, S. Suh, J. Barrett, H.C. de Coninck, C.F. Diaz Morejon, R. Mathur, N. Nakicenovic, A. Ofosu Ahenkora, J. Pan, H. Pathak, J. Rice, R. Richels, S.J. Smith, D.I. Stern, F.L. Toth, and P. Zhou**, “Drivers, Trends, and Mitigation,” in O. Edenhofer, R. Pichs-Madruga, Y. Sokona, E. Farahani, S. Kadner, K. Seyboth, A. Adler, I. Baum, S. Brunner, P. Eickemeier, B. Kriemann, J. Savolainen, S. Schlamer, C. von Stechow, T. Zwickel, and J.C. Minx, eds., *Climate Change 2014: Mitigation of Climate Change. Contribution of Working Group III to the Fifth Assessment Report of the Intergovernmental Panel on Climate Change*, Cambridge University Press, 2014, pp. 351–411.
- Buitenhuis, E.T., T. Hashioka, and C. Le Quéré**, “Combined constraints on global ocean primary production using observations and models,” *Global Biogeochemical Cycles*, 2013, 27 (3), 847–858.
- Canadell, J.G., C. Le Quéré, M.R. Raupach, C.B. Field, E.T. Buitenhuis, P. Ciais, T.J. Conway, N.P. Gillett, R. A. Houghton, and G. Marland**, “Contributions to accelerating atmospheric CO₂ growth from economic activity, carbon intensity, and efficiency of natural sinks,” *Proceedings of the National Academy of Sciences*, 2007, 104 (47), 18866–18870.
- _____, D. Pataki, R. Gifford, R. Houghton, Y. Luo, M. Raupach, P. Smith, and W. Steffen, “Saturation

- of the Terrestrial Carbon Sink,” *Terrestrial Ecosystems in a Changing World*, 01 2007, pp. 59–78.
- Castruccio, Stefano and Joseph Guinness**, “An evolutionary spectrum approach to incorporate large-scale geographical descriptors on global processes,” *Journal of the Royal Statistical Society: Series C (Applied Statistics)*, 2017, *66* (2), 329–344.
- _____, **Michael L Stein et al.**, “Global space–time models for climate ensembles,” *The Annals of Applied Statistics*, 2013, *7* (3), 1593–1611.
- Decharme, B., C. Delire, M. Minvielle, J. Colin, J.-P. Vergnes, A. Alias, D. Saint-Martin, R. Séférian, S. Sénési, and A. Volodire**, “Recent changes in the ISBA-CT RIP land surface system for use in the CNRM-CM6 climate model and in global off-line hydrological applications,” *Journal of Advances in Modeling Earth Systems*, 2019, *11* (5), 1207–1252.
- Denvil-Sommer, A., M. Gehlen, M. Vrac, and C. Mejia**, “LSCE-FFNN-v1: the reconstruction of surface ocean pCO₂,” *Geoscientific Model Development*, 2019, *12*, 2091–2105.
- Dickey, D.A. and W.A. Fuller**, “Likelihood Ratio Statistics for Autoregressive Time Series with a Unit Root,” *Econometrica*, 1981, *49* (4), 1057–1072.
- Slagter, E. and P. Tans**, “Trends in atmospheric carbon dioxide,” Technical Report, National Oceanic and Atmospheric Administration, Earth System Research Laboratory (NOAA/ESRL) 2019. last access: 3 November 2019.
- Doney, S.C., I. Lima, R.A. Feely, D.M. Glover, K. Lindsay, N. Mahowald, J.K. Moore, and R. Wanninkhof**, “Mechanisms governing interannual variability in upper-ocean inorganic carbon system and air–sea CO₂ fluxes: Physical climate and atmospheric dust,” *Deep Sea Research Part II: Topical Studies in Oceanography*, 2009, *56* (8–10), 640–655.
- Doornik, J.A.**, “Autometrics,” in Jennifer Castle and Neil Shephard, eds., *The Methodology and Practice of Econometrics: A Festschrift in Honour of David F. Hendry*, Oxford University Press, 2009, pp. 88–121.
- Durbin, J. and S.J. Koopman**, *Time series analysis by state space methods*, Oxford University Press, 2012.
- Durbin, James and Siem Jan Koopman**, “A simple and efficient simulation smoother for state space time series analysis,” *Biometrika*, 2002, *89* (3), 603–616.
- Feely, R. A., R. Wanninkhof, T. Takahashi, and P. Tans**, “Influence of El Niño on the equatorial Pacific contribution to atmospheric CO₂ accumulation,” *Nature*, 1999, *398* (6728), 597–601.
- Friedlingstein, P., M. Jones, M. O’Sullivan, R. Andrew, J. Hauck, G. Peters, W. Peters, J. Pongratz, S. Sitch, C. Le Quéré et al.**, “Global carbon budget 2019,” *Earth System Science Data*, 2019, *11* (4), 1783–1838.
- Fuller, W.A.**, *Introduction to Statistical Time Series*, John Wiley & Sons, 1996.
- Gifford, R.M.**, “Implications of CO₂ effects on vegetation for the global carbon budget,” in M. Heimann, ed., *The global carbon cycle*, Springer, 1993, pp. 159–199.
- Gilfillan, D., G. Marland, T. Boden, and R. Andres**, “Global, Regional, and National Fossil-Fuel CO₂ Emissions,” <https://energy.appstate.edu/CDIAC> 2019. Accessed: 2019-09-27.
- Gloor, M., J. L. Sarmienti, and N. Gruber**, “What can be learned about carbon cycle climate feedbacks from the CO₂ airborne fraction?,” *Atmospheric Chemistry and Physics*, 2010, *10*, 7739 – 7751.

- Goll, D.S., A.J. Winkler, T. Raddatz, N. Dong, I.C. Prentice, P. Ciais, and V. Brovkin**, “Carbon-nitrogen interactions in idealized simulations with JSBACH (version 3.10),” *Geoscientific Model Development*, 2017, 10, 2009–2030.
- Guinness, Joseph and Dorit Hammerling**, “Compression and conditional emulation of climate model output,” *Journal of the American Statistical Association*, 2018, 113 (521), 56–67.
- Hamilton, J.D.**, “Oil and the macroeconomy since World War II,” *Journal of Political Economy*, 1983, 91 (2), 228–248.
- , “This is what happened to the oil price-macroeconomy relationship,” *Journal of Monetary Economics*, 1996, 38 (2), 215–220.
- , “What is an oil shock?,” *Journal of Econometrics*, 2003, 113 (2), 363–398.
- Hansis, E., S.J. Davis, and J. Pongratz**, “Relevance of methodological choices for accounting of land use change carbon fluxes,” *Global Biogeochemical Cycles*, 2015, 29 (8), 1230–1246.
- Hauck, J., A. Lenton, C. Langlais, and R. Matear**, “The fate of carbon and nutrients exported out of the Southern Ocean,” *Global Biogeochemical Cycles*, 2018, 32 (10), 1556–1573.
- Haverd, V., B. Smith, L. Nieradzik, P.R. Briggs, W. Woodgate, C.M. Trudinger, J.G. Canadell, and M. Cuntz**, “A new version of the CABLE land surface model (Subversion revision r4601) incorporating land use and land cover change, woody vegetation demography, and a novel optimisation-based approach to plant coordination of photosynthesis,” *Geoscientific Model Development*, 2018, 11, 2995–3026.
- Holden, P.B., N.R. Edwards, P.H. Garthwaite, and R.D. Wilkinson**, “Emulation and interpretation of high-dimensional climate model outputs,” *Journal of Applied Statistics*, 2015, 42 (9), 2038–2055.
- Houghton, R.A. and A.A. Nassikas**, “Global and regional fluxes of carbon from land use and land cover change 1850–2015,” *Global Biogeochemical Cycles*, 2017, 31 (3), 456–472.
- IMF**, “International Monetary Fund World Economic Outlook Update: Still Sluggish Global Growth,” <https://www.imf.org/en/Publications/WEO/Issues/2019/07/18/WEOupdateJuly2019> July 2019. Accessed: 2020-10-13.
- , “International Monetary Fund World Economic Outlook: A Crisis Like No Other, An Uncertain Recovery,” <https://www.imf.org/en/Publications/WEO/Issues/2020/06/24/WEOUpdateJune2020> June 2020. Accessed: 2020-10-13.
- Joos, F., I.C. Prentice, S. Sitch, R. Meyer, G. Hooss, G.-K. Plattner, S. Gerber, and K. Hasselmann**, “Global warming feedbacks on terrestrial carbon uptake under the Intergovernmental Panel on Climate Change (IPCC) emission scenarios,” *Global Biogeochemical Cycles*, 2001, 15 (4), 891–907.
- , **M. Bruno, R. Fink, U. Siegenthaler, T.F. Stocker, C. Le Quere, and J.L. Sarmiento**, “An efficient and accurate representation of complex oceanic and biospheric models of anthropogenic carbon uptake,” *Tellus B*, 1996, 48 (3), 397–417.
- Kato, E., T. Kinoshita, A. Ito, M. Kawamiya, and Y. Yamagata**, “Evaluation of spatially explicit emission scenario of land-use change and biomass burning using a process-based biogeochemical model,” *Journal of Land Use Science*, 2013, 8 (1), 104–122.
- Kilian, L.**, “The economic effects of energy price shocks,” *Journal of Economic Literature*, 2008, 46 (4), 871–909.

- , “Not all oil price shocks are alike: Disentangling demand and supply shocks in the crude oil market,” *American Economic Review*, 2009, 99 (3), 1053–69.
- Knorr, W.**, “Is the airborne fraction of anthropogenic CO₂ emissions increasing?,” *Geophysical Research Letters*, 2009, 36.
- Krinner, G., N. Viovy, N. de Noblet-Ducoudré, J. Ogée, J. Polcher, P. Friedlingstein, P. Ciais, S. Sitch, and I.C. Prentice**, “A dynamic global vegetation model for studies of the coupled atmosphere-biosphere system,” *Global Biogeochemical Cycles*, 2005, 19 (1).
- Kwiatkowski, D., P.C.B. Phillips, P. Schmidt, and Y. Shin**, “Testing the null hypothesis of stationarity against the alternative of a unit root: How sure are we that economic time series have a unit root?,” *Journal of Econometrics*, 1992, 54 (1-3), 159–178.
- Landschuetzer, P., N. Gruber, and D.C.E. Bakker**, “Decadal variations and trends of the global ocean carbon sink,” *Global Biogeochemical Cycles*, 2016, 30 (10), 1396–1417.
- Law, R.M., T. Ziehn, R.J. Matear, A. Lenton, M.A. Chamberlain, L.E. Stevens, W. Ying-Ping, J. Srbinovsky, D. Bi, H. Yan et al.**, “The carbon cycle in the Australian Community Climate and Earth System Simulator (ACCESS-ESM1)–Part 1: Model description and pre-industrial simulation,” *Geoscientific Model Development*, 2017, 10 (7), 2567.
- Lawrence, D.M., R.A. Fisher, C.D. Koven, K.W. Oleson, S.C. Swenson, G. Bonan, N. Collier, B. Ghimire, L. van Kampenhout, D. Kennedy et al.**, “The Community Land Model version 5: Description of new features, benchmarking, and impact of forcing uncertainty,” *Journal of Advances in Modeling Earth Systems*, 2019, 11 (12), 4245–4287.
- Lee, C.-C.**, “Energy consumption and GDP in developing countries: A cointegrated panel analysis,” *Energy Economics*, 2005, 27 (3), 415 – 427.
- Lienert, S. and F. Joos**, “A Bayesian ensemble data assimilation to constrain model parameters and land-use carbon emissions,” *Biogeosciences*, 2018, 15 (9), 2909–2930.
- Marland, G. and R.M. Rotty**, “Carbon dioxide emissions from fossil fuels: a procedure for estimation and results for 1950–1982,” *Tellus B: Chemical and Physical Meteorology*, 1984, 36 (4), 232–261.
- Mauritsen, T., J. Bader, T. Becker, J. Behrens, M. Bittner, R. Brokopf, V. Brovkin, M. Claussen, T. Crueger, M. Esch et al.**, “Developments in the MPI-M Earth System Model version 1.2 (MPI-ESM1.2) and its response to increasing CO₂,” *Journal of Advances in Modeling Earth Systems*, 2019, 11 (4), 998–1038.
- Meinshausen, M., S.C.B. Raper, and T.M.L. Wigley**, “Emulating coupled atmosphere-ocean and carbon cycle models with a simpler model, MAGICC6–Part 1: Model description and calibration,” *Atmospheric Chemistry and Physics*, 2011, 11 (4), 1417–1456.
- Meiyappan, P., A.K. Jain, and J.I. House**, “Increased influence of nitrogen limitation on CO₂ emissions from future land use and land use change,” *Global Biogeochemical Cycles*, 2015, 29 (9), 1524–1548.
- Melton, J.R. and V.K. Arora**, “Competition between plant functional types in the Canadian Terrestrial Ecosystem Model (CTEM) v. 2.0,” *Geoscientific Model Development*, 2016, 9 (1), 323.
- Nabeya, S. and K. Tanaka**, “Asymptotic theory of a test for the constancy of regression coefficients against the

- random walk alternative,” *Annals of Statistics*, 1988, 16, 218–235.
- Nyblom, J.**, “Testing for deterministic linear trend in time series,” *Journal of the American Statistical Association*, 1986, 81 (394), 545–549.
- _____ and **T. Mäkeläinen**, “Comparisons of tests for the presence of random walk coefficients in a simple linear model,” *Journal of the American Statistical Association*, 1983, 78 (384), 856–864.
- of East Anglia Climatic Research Unit, University**, “Southern Oscillation Index,” <https://crudata.uea.ac.uk/cru/data/soi/> 2020. Accessed: 2020-10-13.
- Oh, W. and K. Lee**, “Causal relationship between energy consumption and GDP revisited: the case of Korea 1970–1999,” *Energy Economics*, 2004, 26 (1), 51 – 59.
- Ozturk, I.**, “A literature survey on energy–growth nexus,” *Energy Policy*, 2010, 38 (1), 340 – 349.
- Paulsen, H., T. Ilyina, K.D. Six, and I. Stemmler**, “Incorporating a prognostic representation of marine nitrogen fixers into the global ocean biogeochemical model HAMOCC,” *Journal of Advances in Modeling Earth Systems*, 2017, 9 (1), 438–464.
- Perron, P.**, “The great crash, the oil price shock, and the unit root hypothesis,” *Econometrica*, 1989, pp. 1361–1401.
- Phillips, P.C.B. and P. Perron**, “Testing for a unit root in time series regression,” *Biometrika*, 1988, 75 (2), 335–346.
- Piketty, T.**, *Capital in the 21st Century*, Belknap/Harvard, 2014.
- Poulter, B., D.C. Frank, E.L. Hodson, and N.E. Zimmermann**, “Impacts of land cover and climate data selection on understanding terrestrial carbon dynamics and the CO₂ airborne fraction,” *Biogeosciences*, 2011, 8, 2027–2026.
- Pretis, F., J. Reade, and G. Sucarrat**, “Automated General-to-Specific (GETS) regression modeling and indicator saturation methods for the detection of outliers and structural breaks,” *Journal of Statistical Software*, 2018, 86 (3).
- Quéré, C. Le, M.R. Raupach, J.G. Canadell, G. Marland, L. Bopp, P. Ciais, T.J. Conway, S.C. Doney, R.A. Feely, P. Foster, P. Friedlingstein, K. Gurney, R.A. Houghton, J.I. House, C. Huntingford, P.E. Levy, M.R. Lomas, J. Majkut, N. Metzl, J.P. Ometto, G.P. Peters, I.C. Prentice, J.T. Randerson, S.W. Running, J.L. Sarmiento, U. Schuster, S. Sitch, T. Takahashi, N. Viovy, G.R. van der Werf, and F.I. Woodward**, “Trends in the sources and sinks of carbon dioxide,” *Nature Geoscience*, 2009, 2, 831 – 836.
- _____, **R.M. Andrew, P. Friedlingstein, S. Sitch, J. Hauck, J. Pongratz, P. Pickers, J.I. Korsbakken, G.P. Peters, J.G. Canadell et al.**, “Global carbon budget 2018,” *Earth System Science Data*, 2018, 10, 2141–2194.
- _____, _____, _____, _____, **J. Pongratz, A.C. Manning, J.I. Korsbakken, G.P. Peters, J.G. Canadell, R.B. Jackson et al.**, “Global carbon budget 2017,” *Earth System Science Data Discussions*, 2017, pp. 1–79.
- Raupach, M. R.**, “The exponential eigenmodes of the carbon-climate system, and their implications for ratios of responses to forcings,” *Earth System Dynamics*, 2013, 4, 31 – 49.

- _____, **J. G. Canadell, and C. Le Quéré**, “Anthropogenic and biophysical contributions to increasing atmospheric CO₂ growth rate and airborne fraction,” *Biogeosciences*, 2008, *5*, 1601 – 1613.
- _____, **M. Gloo, J. L. Sarmiento, J. G. Canadell, T. L. Frölicher, T. Gasser, R. A. Houghton, C. Le Quéré, and C. M. Trudinger**, “The declining uptake rate of atmospheric CO₂ by land and ocean sinks,” *Biogeosciences*, 2014, *11* (13), 3453–3475.
- Raupach, M.R., G. Marland, P. Ciais, C. Le Quéré, J.G. Canadell, G. Klepper, and C.B. Field**, “Global and regional drivers of accelerating CO₂ emissions,” *Proceedings of the National Academy of Sciences*, 2007, *104* (24), 10288–10293.
- Rayner, P. J., A. Stavert, M. Scholze, A. Ahlström, C. E. Allison, and R. M. Law**, “Recent changes in the global and regional carbon cycle: analysis of first-order diagnostics,” *Biogeosciences*, 2015, *12* (3), 835–844.
- Rödenbeck, C., D.C.E. Bakker, N. Metzl, A. Olsen, C. Sabine, N. Cassar, F. Reum, R.F. Keeling, and M. Heimann**, “Interannual sea–air CO₂ flux variability from an observation-driven ocean mixed-layer scheme,” *Biogeosciences*, 2014, *11*, 4599–4613.
- Ropelewski, C.F. and P.D. Jones**, “An extension of the Tahiti–Darwin Southern Oscillation Index,” *Monthly Weather Review*, 1987, *115*, 2161–2165.
- Schwinger, J., N. Goris, J.F. Tjiputra, I. Kriest, M. Bentsen, I. Bethke, M. Ilicak, K.M. Assmann, and C. Heinze**, “Evaluation of NorESM-OC (versions 1 and 1.2), the ocean carbon-cycle stand-alone configuration of the Norwegian Earth System Model (NorESM1),” *Geoscientific Model Development*, 2016, *9*, 2589–2622.
- Sellar, A.A., C.G. Jones, J.P. Mulcahy, Y. Tang, A. Yool, A. Wiltshire, F.M. O’Connor, M. Stringer, R. Hill, J. Palmieri et al.**, “UKESM1: Description and evaluation of the UK Earth System Model,” *Journal of Advances in Modeling Earth Systems*, 2019, *11* (12), 4513–4558.
- Shephard, N.**, “Distribution of the ML Estimator of an MA(1) and a Local Level Model,” *Econometric Theory*, 1993, *9*, 377–401.
- Smith, B., D. Warlind, A. Arneth, T. Hickler, P. Leadley, J. Siltberg, and S. Zaehle**, “Implications of incorporating N cycling and N limitations on primary production in an individual-based dynamic vegetation model,” *Biogeosciences*, 2014, *11*, 2027–2054.
- Stern, D.I.**, “Energy and economic growth in the USA: A multivariate approach,” *Energy Economics*, 1993, *15* (2), 137 – 150.
- _____, “A multivariate cointegration analysis of the role of energy in the US macroeconomy,” *Energy Economics*, 2000, *22* (2), 267 – 283.
- _____, and **A. Kander**, “The role of energy in the industrial revolution and modern economic growth,” *The Energy Journal*, 2012, *33* (3).
- Stock, J. H. and M. W. Watson**, “Evidence on Structural Instability in Macroeconomic Time Series Relation,” *Journal of Business and Economic Statistics*, 1996, *14* (1), 11–30.
- Tian, H., G. Chen, C. Lu, X. Xu, D.J. Hayes, W. Ren, S. Pan, D.N. Huntzinger, and S.C. Wofsy**, “North American terrestrial CO₂ uptake largely offset by CH₄ and N₂O emissions: toward a full accounting of the greenhouse gas budget,” *Climatic Change*, 2015, *129* (3-4), 413–426.

Walker, A.P., T. Quaife, P.M. van Bodegom, M.G. De Kauwe, T.F. Keenan, J. Joiner, M.R. Lomas, N. MacBean, C. Xu, X. Yang et al., “The impact of alternative trait-scaling hypotheses for the maximum photosynthetic carboxylation rate (V_{cmax}) on global gross primary production,” *New Phytologist*, 2017, 215 (4), 1370–1386.

World Bank, “World GDP (constant 2010 US\$),” <https://data.worldbank.org/indicator/NY.GDP.MKTP.KD> 2020. Accessed: 2020-05-27.

_____, “Global Economic Prospects,” <https://openknowledge.worldbank.org/handle/10986/31655> June 2019. Accessed: 2020-10-13.

_____, “Global Economic Prospects,” <https://openknowledge.worldbank.org/handle/10986/33748> June 2020. Accessed: 2020-10-13.

Zaehle, S. and A.D. Friend, “Carbon and nitrogen cycle dynamics in the O-CN land surface model: 1. Model description, site-scale evaluation, and sensitivity to parameter estimates,” *Global Biogeochemical Cycles*, 2010, 24 (1).

Zhang, X.-P. and X.-M. Cheng, “Energy consumption, carbon emissions, and economic growth in China,” *Eco-logical Economics*, 2009, 68 (10), 2706 – 2712.

(M. Bennedsen) CENTER FOR RESEARCH IN ECONOMETRIC ANALYSIS OF TIME SERIES (CREATES), DEPARTMENT OF ECONOMICS AND BUSINESS ECONOMICS, AARHUS UNIVERSITY, FUGLESANGSALLÉ 4, 8210 AARHUS V, DENMARK.

Email address: mbennedsen@econ.au.dk

(E. Hillebrand) CREATES, DEPARTMENT OF ECONOMICS AND BUSINESS ECONOMICS, AARHUS UNIVERSITY, FUGLESANGSALLÉ 4, 8210 AARHUS V, DENMARK.

Email address: ehillebrand@creates.au.dk

(S.J. Koopman) VRIJE UNIVERSITEIT AMSTERDAM, DEPARTMENT OF ECONOMETRICS, AND CREATES, DE BOELELAAN 1105, 1081 HV AMSTERDAM, THE NETHERLANDS.

Email address: s.j.koopman@vu.nl